Author Manuscript

Author Manuscript

Author Manuscript

Author Manuscript

HHS Public Access

Author manuscript

Pharm Res. Author manuscript; available in PMC 2019 June 30.

Published in final edited form as:

Pharm Res. ; 35(4): 72. doi:10.1007/s11095-018-2362-0.

Human Primary Cell-Based Organotypic Microtissues for Modeling Small Intestinal Drug Absorption

Seyoum Ayehunie[1], **Tim Landry**[1], **Zachary Stevens**[1], **Alex Armento**[1], **Patrick Hayden**[1], and **Mitchell Klausner**[1]

[1]MatTek Corporation, 200 Homer Avenue, Ashland, Massachusetts, USA

Abstract

Purpose—The study evaluates the use of new *in vitro* primary human cell-based organotypic small intestinal (SMI) microtissues for predicting intestinal drug absorption and drug-drug interaction.

Methods—The SMI microtissues were reconstructed using human intestinal fibroblasts and enterocytes cultured on a permeable support. To evaluate the suitability of the intestinal microtissues to model drug absorption, the permeability coefficients across the microtissues were determined for a panel of 11 benchmark drugs with known human absorption and Caco-2 permeability data. Drug-drug interactions were examined using efflux transporter substrates and inhibitors.

Results—The 3D–intestinal microtissues recapitulate the structural features and physiological barrier properties of the human small intestine. The microtissues also expressed drug transporters and metabolizing enzymes found on the intestinal wall. Functionally, the SMI microtissues were able to discriminate between low and high permeability drugs and correlated better with human absorption data ($r^2 = 0.91$) compared to Caco-2 cells ($r^2 = 0.71$). Finally, the functionality of efflux transporters was confirmed using efflux substrates and inhibitors which resulted in efflux ratios of >2.0 fold and by a decrease in efflux ratios following the addition of inhibitors.

Conclusion—The SMI microtissues appear to be a useful preclinical tool for predicting drug bioavailability of orally administered drugs.

Keywords

caco-2; drug-drug interaction; drug metabolizing enzymes; drug permeation; drug transporters; organotypic small intestinal microtissues

INTRODUCTION

It is estimated that more than 60% of marketed drugs are orally administered and 90% of orally administered drug absorption occurs in the small intestine (1). However, currently available *in vitro* 2D–intestine drug screening models are neither organ nor species-specific relying predominantly on the use of cell lines generated from the colon or kidney (as

Seyoum Ayehunie sayehunie@mattek.com.

Author Manuscript Author Manuscript Author Manuscript Author Manuscript

opposed to primary human small intestinal enterocytes). In addition, cell line monolayers or 3-dimensional tissues generated from these cell lines do not mimic the 3D architecture or functionality of the native human small intestine (2) and do not adequately predict gastrointestinal adverse drug reactions (GI ADR) (3). As a result, many drug candidates fail during the preclinical and clinical phases due to insufficient absorption properties (1) and/or induction of GI ADR in humans. These failures are often costly and time-consuming for pharmaceutical companies suggesting the need for translational *in vitro* models that are more predictive of clinical outcomes.

Currently Caco-2 (4) and Madin-Darby canine kidney (MDCK) cell line (5) based single or combination assays are used to understand and predict intestinal drug absorption (6). The Caco-2 cell-based cultures are considered the gold standard for drug absorption studies even though they form a non-physiological barrier due to paracellular junctions that are much tighter and less permeable than the native human intestinal epithelium. Transepithelial electrical resistance (TEER) measurements for Caco-2 monolayers/tissues range from 250 to 2400 $\Omega*cm^2$ compared to TEER values of 12–120 $\Omega*cm^2$ for human small intestinal tissue (7). These elevated barrier properties are due to the fact that the Caco-2 lines originated from colon and also have an average tight junction pore radius of 3.7 Å, compared to 8–13 Å for native human tissue (8). Caco-2 cells also have other limitations such as: a) weak expression of important intestinal metabolic enzymes such as cytochrome P450 (CYP)3A (9), b) lack of the crypt-villus axis which is important for fluid and ion transport, c) absence of mucus producing cells, and d) variability in cell line and clone selection, which can lead to 20-fold differences in TEER from laboratory-to-laboratory (10). The intestinal barrier has also been modeled using MDCK cells (6). However, MDCK are of dog kidney origin and produce monolayer cultures that are less permeable barrier than human small intestinal tissue (e.g. TEER values range from 300 to 4000 Ω (Ω)$*cm^2$,6). Also, the main efflux transporter, P-gp, which impacts drug bioavailability, is poorly expressed in these cell lines.

Other models used to mimic the human small intestine include organoids produced from primary intestinal stem cells, human explant tissues, and laboratory animals. Organoid based models have advanced our understanding of the basic biology of the intestinal organ. However, organoids are spherical and are embedded in a Matrigel matrix, and thus they are not suitable for drug permeation or efflux experiments (11). Human intestine explant cultures have been used for drug permeation studies, but the scarcity of normal human tissue and their short survival time ex vivo make their use infeasible for meeting the needs of modern day drug development programs. Animal models also have fundamental problems since they are expensive, are low throughput, and do not adequately recapitulate human physiology (12) due to species differences. Therefore, cost-effective, high throughput, organotypic intestinal microtissues which are physiologically relevant would be of great utility to the pharmaceutical industry for optimizing compounds and compound formulations and predicting bioavailability of orally administered drugs at an early stage of drug development (11).

The development of a human primary cell-based tissue model to accurately predict drug safety and permeation remains a major challenge for the pharmaceutical industry (13). In this study, we developed and characterized a new organotypic 3D human small intestinal

Author Manuscript Author Manuscript Author Manuscript Author Manuscript

(SMI) microtissue model which closely mimics native human small intestine tissue. The geometry of the SMI microtissue is distinct from intestinal organoids and is closely aligned with the polarized nature of the intestinal tissue, thereby allowing bidirectional drug transport through the intestinal wall (apical to basolateral and vice-versa). Advantages of the 3D–small intestinal microtissues include the use of primary cells of human intestinal origin, tissue polarization, and the expression of drug transporters similar to native SMI tissue. These attributes make them ideal for studies involving: a) bidirectional drug transport (apical (A) to basolateral (B) or B-to-A), b) pre- and post-drug exposure barrier measurements (TEER), c) drug-drug interaction, and d) drug metabolism studies.

The Food and Drug Administration (FDA) and other regulatory agencies apply the Biopharmaceutical Classification System (BCS) guidelines to justify the use of *in vitro* solubility and permeability data in order to waive the need for expensive bioequivalence clinical studies of high solubility and high permeability drugs (14, 15). The BCS classifies drugs as: Class 1 (high solubility, high permeability), Class 2 (low solubility, high permeability), and Class 3 (high solubility, low permeability), and Class 4 (low solubility, low permeability). In this study, we extensively characterized the barrier function, drug transporters and drug metabolizing enzyme expression in the SMI microtissues. We also extensively characterized the bidirectional transport of 11 model drugs and compared the permeation of drugs from different BCS categories using the reconstructed SMI microtissues to Caco-2 monolayer and historical data for human absorption.

MATERIALS AND METHODS

Cell Source

Human small intestine cells were obtained either from commercial sources as previously described (16) or isolated from tissues obtained from the International Institute for the Advancement of Medicine (IIAM; Scranton, PA) through the Organ Procurement Organization (OPO). All tissue specimens were collected from brain-dead donors with informed consent from the next of kin. Samples were protected from ischemic injury by flushing with ice-cold University of Wisconsin storage solution immediately after vascular clamping and resection. Epithelial cells and fibroblasts were isolated from ileum, jejunum, or duodenum. Cells were expanded and cryopreserved for future use. In this study, SMI microtissues were cultured using cells obtained from the ileum region of the small intestine from a 19-year-old female donor. The primary intestinal fibroblasts were purchased from Lonza (Walkersville, MD).

Reconstructed Small Intestinal and Caco-2 Microtissues

To reconstruct the 3D small intestinal microtissues, cryopreserved fibroblasts were thawed, expanded in DMEM supplemented with 10% fetal bovine serum, trypsinized, counted and seeded (3.0×10^5 cells/cm^2) onto collagen coated cell culture inserts (MatTek Corporation, 0.6 cm^2) or into a high throughput, membrane bottom 96-well plate (Millipore Corporation, 0.12 cm^2/well). The fibroblasts were incubated at 37°C for 4–6 h and primary human small intestinal epithelial cells were seeded and cultured in a proprietary medium formulation (SMI-100-FT-MM, MatTek Corporation, Ashland, MA) for 4 days submerged, and for an

Author Manuscript Author Manuscript Author Manuscript Author Manuscript

additional 10 days at the air–liquid interface (ALI) at 37°C, 5% CO_2 and 98% relative humidity. During the ALI culture period, these tissues (designated SMI-100-FT or EpiIntestinal-FT) were fed basolaterally through the membrane of the cell culture inserts or the 96-well plate. Some experiments utilized epithelial microtissues (designated as SMI-100 or EpiIntestinal-PT) in which only epithelial cells were seeded directly onto the collagen coated membrane bottom 96-well plates (i.e. fibroblasts were not included in the model). Caco-2 cells (passage 40–60) were cultured in 96-well membrane bottom plates at 37°C, for 20 days at Cyprotex (Watertown, MA), as per previously established methods (17).

Test Compounds

The model drugs tested in this study were purchased from Sigma Aldrich Corp. (Sigma Aldrich, St Louis, MO, USA) except where otherwise noted (Table I). The drugs represent a diverse range of physicochemical properties. Prior to permeability studies, the SMI microtissues were exposed to various drug concentrations to ensure that they were not toxic. All drugs were initially tested at three concentrations (1 μM, 10 μM, and 100 μM) and SMI microtissue viability was determined using the MTT assay following 2× exposures (0 and 48 h) for 96 h. The median concentration of 10 μM was subsequently chosen for all drug permeation studies since this concentration is non-cytotoxic and commonly utilized for drug permeation testing in Caco-2 studies (personal communication from Cyprotex).

Characterization of the SMI Microtissues

Histology—The reconstructed SMI microtissues were fixed with 10% formalin overnight. The tissues were embedded in paraffin and cross-sections were cut (5–7 mm thick), stained with H&E, and photographed using an Olympus VS 120 microscope.

Tissue Viability (MTT Viability Assay)—Viability of the microtissues was determined using the MTT assay. The extent to which MTT is reduced to a purple formazan dye has been correlated to cell viability (18). After exposure of the microtissues tissues to the test drug or positive control, the microtissues were rinsed with PBS and then loaded with MTT (3-(4,5-dimethylthiazole-2-yl)-2,5-diphenyl tetrazolium bromide; Sigma). Loading of MTT was accomplished by placing the microtissues into a 96-well receiver tray containing 100 μL/well of MTT dye (1 mg/mL) in culture medium. The plates were placed into a 37°C, 5% CO_2 incubator for 3 h. After 3 h, the MTT solution remaining in the 96-well receiver tray was discarded and replaced with 250 μL/well of MTT extractant solution (isopropyl alcohol). Additionally, 150 μL of the extractant was added to the top (apical) surface of each microtissue. The plate was sealed in a plastic bag and the extraction was allowed to proceed overnight at room temperature in the dark. Afterwards, 200 μL of the formazan extract was quantified by measuring optical density (OD) at 570 nm in an E-MAX 96-well plate reader (Molecular Devices, Menlo Park, CA). The viability of the microtissues was determined by normalizing the OD for treated tissues as a percent of the negative control (untreated) microtissues.

Protein Expression—Immunohistochemistry was used to detect the expression of specific intestinal markers within the SMI microtissues including cytokeratin (CK)-19 (marker for epithelial cells), ZO-1 (marker for tight junctions), villin (marker for brush

Author Manuscript Author Manuscript Author Manuscript Author Manuscript

borders), and vimentin (marker for fibroblasts). 5-μm-thick paraffin sections were mounted on glass slides, deparaffinized, and rehydrated using a graded series of ethanol. Slides were processed for antigen retrieval by heating in a citrate buffer (pH 7.4) for 45 min at 95–99°C. After 45 min, the specimens were removed from the water bath and left in the citrate buffer for an additional 20 min at room temperature (RT). Antibodies for the cytokeratin CK19 (2 μg/mL, cat# ab7754, Abcam, Cambridge, MA), tight junction protein, ZO-1 (1 μg/mL, cat# 61–7300, Life Technologies, Carlsbad, MA), brush border marker, villin (2 μg/mL, cat# ab97512, Abcam, Cambridge, MA), and fibroblast marker, vimentin (50 μg/mL, cat# ab24525, Abcam, Cambridge, MA), and p-glycoprotein (P-gp; Abcam Catalogue# ab170904) were used. Primary antibodies were applied for 60 min at RT. Antibodies were visualized using AlexaFluor® secondary antibodies (5 μg/mL, Life Technologies, Carlsbad, CA). DAPI (cat# D1306, Life Technologies, Carlsbad, CA) was used for nuclear staining. All images were captured using a FV1000 confocal microscope (Olympus America Inc., Center Valley, PA).

Ultrastructural Features—To examine the ultrastructural features of the SMI microtissues, transmission electron microscopy (TEM) and scanning electron microscopy (SEM) were used, following procedures as previously described (19). Briefly, tissues were fixed at room temperature for 2 h using 5% glutaraldehyde in 0.1 M sodium cacodylate buffer, pH 7.2 and post-fixed with 1% Osmiumtetroxide (OsO_4)/1.5% Potassium ferrocyanide($KFeCN_6$) for 1 h. Samples were washed in water (2×) and in 50 mM Maleate buffer pH 5.15 (MB) (1×), incubated in 1% uranyl acetate in MB for 1 h, and again washed in MB and water. Samples were dehydrated in a graded series of ethanol, put in propyleneoxide for 1 h, and infiltrated with a 1:1 mixture of propyleneoxide and TAAB Epon (Marivac Canada Inc., St. Laurent, Canada). Ultrathin sections (80 nm) were cut, picked up on to copper grids stained with lead citrate and examined using a JEOL 1200EX Transmission electron microscope at Harvard Medical School (Boston, MA). For SEM, following dehydration the samples were critically point dried and mounted onto specimen mounts using double sided carbon conductive adhesive. Samples were sputter coated with 5 nm platinum using a Cressington 208 HR sputter coater. Samples were viewed on a Hitachi S-4800 FESEM at Northeastern University (Boston, MA). Techniques described above were used to visualize ultrastructural features including the villi, brush borders, and tight junctions in the SMI microtissues.

Barrier Integrity—Changes in barrier function of the SMI microtissues were quantified using transepithelial electrical resistance (TEER) measurements. TEER monitors the presence of functional intercellular tight junctions which are responsible for the barrier function in SMI tissue. TEER measurements were made using the EVOM volt-ohmmeter equipped with an EndOhm electrode chamber (World Precision Instruments, Sarasota, FL). Raw resistance measurements (Ω) were converted to TEER readings ($\Omega*cm^2$) by multiplying the raw readings for each tissue by the surface area of the cell culture inserts(0.6 cm^2) or the 96-well membrane bottom plate (0.12 cm^2). TEER measurements were normalized as a percentage of the untreated control tissues: % TEER = TEER ($\Omega*cm^2$) of treated tissues (TTT) divided by the TEER of untreated tissues (TUT) times 100 (% TEER = (TTT/TUT)*100.

Author Manuscript Author Manuscript Author Manuscript Author Manuscript

Lucifer Yellow Leakage Assay—Changes induced to the barrier function of the microtissues by the model drugs were monitored using the Lucifer Yellow (LY) leakage assay. LY transits through the intestinal tissue exclusively by paracellular diffusion and has low permeability in intact epithelium. Therefore, the barrier integrity of the drug treated tissues was measured by co-applying the test drug with 100 μM Lucifer (LY) dye to the donor side buffer. At the end of the 2 h permeation experiment, the LY concentration in the receiver solution was determined using a fluorescence plate reader (Synergy HT, Multi-Detection Microplate reader, Winooski, VT) at 485/535 nm. The LY permeation from the apical to the basolateral wells after 2 h of exposure to the model drugs was normalized to the LY that permeated through inserts without any tissues. Tissue barrier integrity was considered intact if LY leakage was <4%.

Ribonucleic Acid (RNA) Isolation and Quantification—Microtissues ($N = 2$) were rinsed three times with phosphate buffered saline and, together with the underlying membrane, cut from the 96-well plate using a scalpel, and deposited into a microfuge tube with lysis/binding buffer (Ambion RNAqueous kit, Ambion Inc., Austin TX). Tissues were homogenized using a pellet pestle and total RNA was isolated following the manufacturer's recommendations. Trace DNA contamination was removed using DNA-*free*™ (Ambion). RNA concentrations were determined using spectrophotometry at 260 nm and the purity was verified using the 260/280 nm ratio. This procedure yielded between 1–2 μg of high quality total RNA per/microtissue (96-well plate format; surface area = 0.12 cm^2). RNA was stored at −80°C until use.

Reverse Transcription Polymerase Chain Reaction (RT-PCR)—To investigate gene expression levels of efflux drug transporters, p-glycoprotein (MDR1), multidrug-resistance associated protein (MRP)-1 and 2, and the breast cancer resistance protein (BCRP), reverse transcriptase-polymerase chain reaction (RT-PCR) was performed using specific primer pairs (20) synthesized by IDT Technologies (Coralville, Iowa). Total RNA (130 ng) isolated from intestinal microtissues was reverse transcribed using the SuperScript® II One-step Reverse Transcription Polymerase Chain Reaction (RT-PCR) system with Platinum® Taq DNA polymerase (Invitrogen, Carlsbad, California) following the manufacturer's recommendations. The thermal cycler was programmed so that complementary DNA (cDNA) synthesis was followed immediately by PCR amplification. The cDNA synthesis was performed by incubating samples with RT-PCR master mix and reverse transcriptase enzyme at 70°C for 10 min, followed by incubation at 42°C for 1 h. This protocol was chosen to minimize nonspecific product amplification). All primer pairs were synthesized at IDT Technologies (Coralville, IA). The PCR program utilized 40 cycles of 1-min duration at 94°C (denaturation), 1 min at 58°C (annealing temperature), and 1 min at 72°C (extension), followed by a final extension at 72°C for 10 min and a hold temperature of 4°C. Glyceraldehyde-3-phosphate dehydrogenase (GAPDH) was used as the amplification internal control. After PCR, the products were resolved on a 2% agarose gel and stained with ethidium bromide. The images were captured using an Ultraviolet transilluminator.

The specific primer pairs used were:

Author Manuscript Author Manuscript Author Manuscript Author Manuscript

P-gp:	Forward	5`-CTGTATTGTTTGCCACCACGA-3`
	Reverse	5`-AGGGTGTCAAATTTATGAGGCAGT-3`
MRP1	Forward	5`-GGGCTGCGGAAAGTCGT-3`
	Reverse	5`-AGCCCTTGATAGCCACGTG-3`
MRP2	Forward	5`-ACTGTTGGCTTTGTTCTGTCCA-3
	Reverse	5`-CAACAGCCACAATGTTGGTCTCTA-3`:
BCRP	Forward	5`-CAGGTCTGTTGGTCAATCTCACA-3`
	Reverse	5`-TCCATATCGTGGAATGCTGAAG-3`

Quantitative Polymerase Chain Reaction (qPCR)—To determine levels of Phase I and II drug metabolizing enzymes, quantitative polymerase chain reaction (qPCR) was performed using a custom RT^2 Profiler PCR array containing pre-plated primers supplied by the manufacturer (Qiagen, Germantown, MD); catalogue numbers for the pre-plated primers are shown in Tables II and III). cDNA was generated using 500 ng total RNA. qPCR was performed by adding12.5 μL of RT^2 SYBR Green qPCR Mastermix, 1 μL of4.5 ng/μL cDNA, and 10.5 μL of sterile water to RT^2 Profiler PCR array containing pre-plated primer pairs. The reaction profile consisted of 10-min incubation at 95°C, followed by 40 cycles of 15 s at 95°C and 60 s at 60°C with a ramp rate of 1°C/s. Quantification of the qPCR products was performed using the Ct (threshold cycle) method, assuming equal amplification efficiencies. The Ct values of the amplified genes were normalized to the Ct values of GAPDH. Genes detectable below 30 PCR cycles (Cq) were considered to be expressed by the microtissues. Analyses of the qRT-PCR data were performed using the BioRad CFX Manager software.

Quality Control—To monitor the suitability of each preparation of SMI microtissues for drug permeability experiments, quality assurance specifications were established. TEER measurements and the Lucifer Yellow (LY) leakage assay were utilized to insure reproducible tissue barrier property. TEER measurements of 70–200 $\Omega*cm^2$ and LY leakage <4% were set as acceptance criteria for the microtissues.

Reproducibility of the In Vitro Microtissues—To investigate reproducibility of the SMI microtissues, tissue-to-tissue variability within a given lot (intra-lot variability) and lot-to-lot variability (inter-lot variability) was determined using TEER, LY leakage, and histology as endpoints. Intra-lot variability was assessed by preparing three replicate tissues that were cultured using cells obtained from a single donor and inter-lot variability was determined by comparing results from 2 to 5 tissue lots cultured with cells obtained from a donor. In addition, the effect of extended culture on tissue barrier integrity was monitored by measuring TEER for up to 42 days (6 weeks). Throughout the 42-day culture period, tissues in the 96-well plate format were fed every other day with apical (20 μL/well) and basolateral (250 μL/well) maintenance medium (MatTek Corporation).

Author Manuscript Author Manuscript Author Manuscript Author Manuscript

Drug Permeation

Drug Permeability Experiments—Drug permeability experiments were performed using the SMI microtissues cultured in a 96-well plate format. The microtissues were shipped to Cyprotex and upon arrival, the microtissues were placed into 96-well trays containing 250 μL of pre-warmed assay medium and equilibrated to 37°C, 5% CO_2 for 24 h. After 24 h, tissues were used for drug permeation studies dosed either apically or basolaterally with test drug (10 μM, diluted in transport buffers). The apical (A)-side transport buffer (donor side buffer) was prepared by adding1.98 g of glucose and 10 mL of 1 M HEPES buffer to 1 L of 1× Hank's Balanced Salt Solution and the pH was adjusted to pH 6.5 (to mimic the lumen side of the intestine). The basolateral (B) to apical (A) transport buffer (receiver side buffer) was identical to the apical side buffer except the pH was adjusted to 7.4 (to mimic the blood side of the intestine). For apical to basolateral (A-to-B) flux experiments, 75 μL of A-side transport buffer containing 10 μM of test article were topically added to the tissues which were in contact with 250 μL of the B-side transport buffer. For basolateral to apical (B-to-A) flux experiments, 10 μM of test article was added to 250 μL of B-side transport buffer and the apical tissue surface was in contact with 75 μL of A-side transport buffer. The dosed tissues are incubated for 2 h at 37°C/5% CO_2. At the end of the 2 h incubation time, samples from the basolateral(B) or apical (A) receiver solutions were collected for A-B or B-A drug permeation, respectively, and the drug concentration in the samples were analyzed using LC-MS/MS system at Cyprotex (Watertown, MA). Since many drug compounds are soluble in DMSO, 75 μL of transport buffer containing DMSO (0.1%) were topically applied to tissues to serve as the vehicle control. Parallel drug permeability experiments were performed using Caco-2 monolayers prepared by Cyprotex.

Liquid Chromatography - Mass Spectrometry (LC/MS)—The samples of donor and receiver side transport buffers from the permeability experiments were analyzed using LC/MS/MS. All analyses were performed using an Agilent 6410 mass spectrometer coupled with an Agilent 1200 HPLC and a CTC PAL chilled autosampler, all controlled by MassHunter software (Agilent) at Cyprotex (Waltham, MA). Analytes were separated on a C18 reverse phase HPLC column (Zorbax Stable Bond 3.5 μM; 2.1 × 3 mm HPLC column, (Agilent, Santa Clara, CA) using an acetonitrile-water gradient system. The drugs were loaded onto the separation column (Zorbax Stable Bond 3.5 μM; 2.1 × 3 mm HPLC column) with 98% solvent A (0.1% formic acid), and 2% solvent B (2% acetonitrile and 0.1% formic acid) at flow rate of 1 μL/min. The instrument settings were as follows: drying gas temperature, 350°C; drying gas flow, 11 L/min; nebulizer pressure, 50 psi; capillary voltage, 4000 V. Using this instrument, a precursor ion is selected using the first quadrupole and is sent to the collision cell for fragmentation. The fragments are scanned through the third quadrupole resulting in a product-ion scan MS/MS. An MS dwell time of 20 msec was used for each multiple reaction monitoring (MRM) transition. Peaks were analyzed by mass spectrometry (MS) using ESI ionization in MRM mode (Table VI).

Metabolic Activity—To examine the metabolic activity of the intestinal microtissues, we used isozyme-specific Vivid™ CYP450 Screening Kits (Life Technologies, Carlsbad, CA) which contain substrates that can be metabolized by specific CYP450 isozymes into

Author Manuscript Author Manuscript Author Manuscript Author Manuscript

products that are highly fluorescent in aqueous solution. The intestinal microtissues were transferred into wells containing 200 μL of CYP450 Reaction Buffer II. Then 180 μL of master-mix of Vivid regeneration system (glucose-6-phosphate and glucose-6-phosphate dehydrogenase) diluted in appropriate buffer was added topically to each tissue and incubated for 10 min at room temperature. After 10 min, 10× Vivid Substrate and Vivid NADP+ mixture (20 μL) was applied topically to each intestinal microtissue (N = 3 tissues per P450 enzyme tested) to initiate the enzymatic reaction (all reagents used were supplied with the Vivid P450 Screening Kit). After exposure for 1, 2, and 3 h, the reactions were stopped using 0.5 M Tris-base and the solution from the apical side of the microtissues was collected for analysis. The fluorescent metabolites were quantified using a fluorescent plate reader (490/520 nm for CYP2C9, CYP3A4, and CYP3A5 and 415/460 nm for CYP2C19). The Vivid® CYP450 assay was performed following the manufacturer's recommendation.

Data Analysis—The apparent permeability coefficient (P_{app}) was calculated according to the equation:

$$P_{app} = (dQ/dt)/\left(C_0 x A\right)$$

where dQ/dt is the rate of permeation, C_0 is the initial concentration of test agent, and A is the area of the monolayer or tissue (A = 0.12 cm^2 for the 96-well format microtissues). In bidirectional permeability studies, the Efflux Ratio (R_e) was also calculated as per: $R_e = \frac{P_{app}(B \rightarrow A)}{P_{app}(A \rightarrow B)}$ indicates a substrate for P-gp or another efflux transporter.

RESULTS

Tissue Phenotype and Characterization

Phenotypic and Structural Features—Cryopreserved primary human intestinal epithelial cells and fibroblasts were expanded in monolayer culture (Fig. 1) and seeded into single-well cell culture inserts or into a high throughput 96-well membrane bottom plate and cultured at the air liquid interface (ALI) to produce 3D–intestinal microtissues. Histological (Fig. 2) and fluorescent microscopic imaging (Fig. 3a–c) of the reconstructed small intestinal microtissues showed *in vivo*-like tissue architecture consisting of an epithelial layer with columnar and villi structures that are positive for cytokeratin-19 (CK-19, epithelial cell marker), villin (a brush border differentiation marker), and vimentin (a fibroblast marker) (Fig. 3a). The reconstructed SMI microtissues also constitutively expressed de novo synthesized extracellular-matrix proteins such as collagen IV and fibronectin (Fig. 3b, c). Similar protein expression was observed in SMI explant control tissues (Fig. 3d). Ultrastructural analysis of the SMI microtissues showed brush border structures conspicuously present on the apical surface that are very similar those of explant small intestinal tissue (Fig. 4a, b). Scanning electron microscopic examination of the microtissues also confirmed brush border formation on the villi (Fig. 4c). The presence of villi and microvilli/brush border in the small intestine increases its surface area for absorption of drugs and other molecules. Furthermore, immunohisto-chemical staining of the tissue revealed the presence of the p-glycoprotein (P-gp) drug transporter on the apical

Author Manuscript Author Manuscript Author Manuscript Author Manuscript

surface of the microtissues (Fig. 5a) overlapping with the brush border. P-gp staining of explant intestinal tissue was used as a control (Fig. 5b).

Transepithelial Electrical Resistance (TEER) and Lucifer Yellow (LY) Leakage—The range of TEER values for ex vivo human SMI tissue is reported to be 12–120 Ω*cm^2, which is significantly lower than the TEER 250–2400 Ω*cm^2 reported for Caco-2 cultures (21). In this study, we developed culture conditions that produce SMI microtissues with columnar epithelium and TEER values of 70–200 Ω*cm^2, which are similar to the *in vivo* physiological range. The average TEER value for the 96-well SMI microtissues over $n = 33$ lots was 152.5 ± 39 Ω*cm^2. LY leakage was also evaluated as a secondary measure of barrier function. The average LY leakage was 0.3% ± 0.05 (data not shown).

Extended Culture Period of the SMI Microtissues—To examine the longevity of the SMI microtissues, the microtissues were cultured for up to 42 days. The microtissues were fed every 48 h with fresh media the apical tissue surface was rinsed with 400 μl of PBS (pH adjusted to 6.5) once a week to remove terminally differentiated and sloughed off epithelial layers that *in vivo*, would normally wash off into the intestinal lumen every 3–5 days. Utilizing this protocol, the barrier integrity of the SMI microtissues was maintained over a 6-week culture period with TEER values ranging from 130 to 192 Ω*cm^2 (Fig. 6).

Expression of Drug Transporters and Drug Metabolizing Enzymes—Since drug transporters (e.g. P-gp) and drug metabolizing enzymes (e.g. CYP3A4) can influence the amount of bio-active drug that permeates from the intestinal lumen into the serosa layer of the gut (22, 23), expression levels of drug transporters and metabolizing enzymes in the SMI microtissues were examined. In this study, we investigated the key efflux transporters including ABCB1/MDR1 (P-glycoprotein, P-gp), ABCC1 (multidrug resistance protein (MRP)-1), ABCC2 (MRP-2), and ABCG2 (breast cancer multidrug resistance protein, BCRP) and the main drug metabolizing enzymes known to be present such as CYP3A4, CYP3A5, and CYP2C9. RT-PCR results showed that the 3D intestinal microtissues express the major efflux drug transporters known to be present in human small intestine (Fig. 7a–c and Table IV). Results also showed that the epithelial layer of the microtissues is responsible for the expression of BCRP, MRP1, and MRP2 since the fold change in expression level is <2 indicating very little biological difference between these microtssues for these three transporters (Table IV). However, expression of P-gp/MDR1 showed a significant upregulation regulation (11.8 fold) suggesting a cross-talk between epithelial cells and fibroblasts. The implication of this change will be investigated in future studies.

Likewise, the most prominent drug metabolizing enzymes known to be present in *in vivo* human SMI were expressed (Table I). In addition, the intestinal microtissues expressed glutathione *S*-transferases, which are Phase II detoxification enzymes, at levels similar to the expression levels of the naive intestinal tissue (Table III). In addition to directly affecting the amount of bio-active drug that is delivered into the bloodstream through the intestinal wall, expression of these efflux transporters and drug-metabolizing enzymes can play an essential role in protecting tissues from xenobiotics and carcinogens (24).

Author Manuscript Author Manuscript Author Manuscript Author Manuscript

Determination of Toxicity of Model Drug Compounds—Prior to drug permeation experiments, cytotoxicity screening of test compounds was performed using TEER measurements, MTT viability, and LY leakage assays. Concentrations were deemed non-toxic using the following criteria: MTT Viability >75%, TEER value >75%, and LY leakage <4% following a 24 h exposure time. Preliminary cytotoxicity experiments were performed utilizing drug concentrations of 1, 10, and 100 μM. At these three concentrations, all drugs were found to be nontoxic. TEER, MTT and LY Leakage data for the test compounds are summarized in Table I.

Drug Permeation Experiments—The ability to accurately predict the absorption of orally administered drugs in the gastrointestinal tract is important for drug bioavailability studies and to appropriately assign dose regimens for patients. One of the advantages of the SMI microtissues is that the tissues have a distinct apical (A) and basolateral (B) side which allows evaluation of A → B (mimicking luminal to bloodstream permeation *in vivo*) or B → A drug transport (bloodstream to lumen). A schematic diagram of drug permeation in SMI tissue is shown in Fig. 8. Initially, we evaluated the utility of the SMI microtissues for rank-ordering the permeability of three model drugs representing low (< 50%, Talinolol), moderate (50–84%, Ranitidine), and high (≥ 85%, warfarin) absorption in humans (25). The results were compared to drug permeation data obtained from the *in vitro* standard, Caco-2 cells, and historical data of % dose absorbed in humans (26, 27) (Table V). As shown, the SMI microtissues appeared to be more predictive of human absorption since Caco-2 cells do not discriminate between Talinolol and Ranitidine while permeation in SMI microtissues scales with human absorption. Based on these results, the ability of the SMI microtissues to predict human absorption was further tested using an expanded set of 11 model drugs. The compounds tested included drugs with low, moderate, and high absorption in humans, as recommended by FDA (27–29). The SMI microtissues correlated very well with the historical human absorption data ($R^2 = 0.91$). The correlation coefficient for parallel permeation experiments using Caco-2 microtissues was $R^2 = 0.71$ (Table VI and Fig. 9).

Drug-Drug Interactions (DDI)—The suitability of the SMI microtissues for drug permeation experiments was further tested using model drugs which are substrates for intestinal efflux transporter substrates (B → A permeability). Permeability experiments were performed to measure P_{app} (A → B) and P_{app} (B → A) and the Efflux ratio (R_e) was calculated. These results were compared to identical experiments in the presence of the efflux transporter inhibitors. In the absence of transporter inhibitors, the R_e for Talinolol (transporter: P-gp), Loperamide (transporter: P-gp), Rosuvastatin (transporter: P-gp), and Nitrofurantoin (transporter: BCRP) was >2 indicating potential involvement drug transporters in the SMI microtissues. However, upon addition of inhibitors to the transporters, the bioavailability of the drugs increases as evidenced by decreased R_e for each drug (Table VII and Fig. 10).

Drug Metabolism—Intestinal permeability and metabolism are key components in the assessment of oral drug absorption. To examine the functionality of drug metabolizing enzymes on the intestinal microtissues, metabolism experiments were performed using two drugs, Midazolam and Fosphenytoin (a phosphate ester prodrug), that are metabolized by

Author Manuscript Author Manuscript Author Manuscript Author Manuscript

CYP3A4 and tissue phosphatases, respectively. Following exposure of the SMI microtissues to the drugs (10 μM of either Midazolam or Fosphenytoin for 2 h), donor and receiver buffers were collected and analyzed using LC/MS/MS. When applied topically (A-B exposure), 6.5% of the parent drug Midazolam was converted to its metabolite, alpha-hydroxy-midazolam, and 57.2% of the parent drug Fosphenytoin was converted to its metabolite, Phenytoin (Table VIII). Furthermore, relevant physiological activity by CYP450 drug metabolizing enzymes (CYP2C9, CYP2C19, CYP3A4, and CYP3A5) expressed on the intestinal microtissues was observed using isozyme-specific fluorogenic substrates of CYP450 enzymes (Fig. 11).

Reliability of the SMI Microtissue Based Drug Permeation Model—The utility of an *in vitro* method critically depends on its short and long-term reproducibility. The human SMI microtissue model must meet performance standards to insure assay reproducibility and validity over extended periods of time. To evaluate the reproducibility of the SMI microtissue model, experiments were repeated using four model drugs and three independent preparations of SMI microtissues. As shown in Table IX, good reproducibility was observed in terms of P_{app} values. All four model drugs tested in the different SMI microtissue preparations were correctly rank ordered from low to high permeability using P_{app} values of A to B transport (bioavailability):

Invitro **tissue model results**: Atenolol

< Ranitidine; Hydrochlorothiazide < Warfarin

Human absorption (%): Atenolol < Ranitidine< Hydrochlorothiazide < Warfarin

DISCUSSION

To perform reliable absorption experiments for orally administered drugs, *in vitro* models should accurately reflect the structure, membrane transport systems, and metabolic pathways of native human intestinal tissue. The intestinal microtissues described in this paper contain enterocytes, Paneth cells, tuft cells, and Muc 2 positive cells and have villi-like structure with brush borders similar to *in vivo* tissue. Formation of villi (finger-like projections) and microvilli (hair like projections) are key anatomical features of the small intestine. The villi and microvilli increase the intestinal surface area and enhance surface absorption by 30–600 fold, respectively (30) and they play a significant role in nutrient and drug processing, solute transport, and host defense (31). The well polarized geometry of the intestinal microtissues which parallels the *in vivo* intestinal epithelial phenotype may contribute to a better prediction of drug absorption, as later discussed.

Quantitative techniques such as physiologically relevant TEER measurements have been developed to assess the barrier integrity of the microtissues before proceeding with drug testing. *In vivo*, at least 22 enzymes and 19 transporters have been reported to be localized in the brush border of the small intestine (32), many of which are expressed in the microtissues (Tables II and III). Development of *in vitro* 3D human primary cell based intestinal microtissues with these key structural, transport, and metabolic features is an advancement over the existing *in vitro* cell based assays.

Author Manuscript Author Manuscript Author Manuscript Author Manuscript

The presence of distinct apical and basolateral surfaces is advantageous for drug permeation studies compared to other *in vitro* culture methods such as organoids. Although intestinal organoid culture systems have been important in the study of stem cell differentiation and disease, their major limitations relate to cyst-like morphology, no defined size, and the closed system of epithelial growth in which the epithelial cells surround a hollow lumen (33). This closed system limits access to the apical tissue surface and make them impractical for drug permeation studies. In contrast, the small intestinal microtissues used in this study have the appropriate morphological features and function that resembles the *in vivo* counterpart with a distinct apical and basolateral surface ideal for modeling lumen to bloodstream (A-to-B) or bloodstream to lumen (B-to-A) transport.

The SMI microtissues have both the epithelial and fibroblast component of the small intestine which allows cross-talk between the two cell types. The small intestinal microtissues produce de novo extracellular matrix (ECM) proteins including collagen IV and fibronectin (Fig. 3) which are important in the 3D microenvironment and influence cellular adhesion, morphogenesis, stem cell differentiation, and maintenance of the epithelium (34, 35). Additional advantages of the SMI microtissues are that they can be cultured in different size formats including 6-well, 12-well and 24-well individual inserts as well as 96-well high-throughput, automation-compatible plates. Recreating 3D microtissues that bridge the gap between 2D *in vitro* and *in vivo* studies is critical to the drug discovery and development process. The availability of a small intestinal microtissue model that mimics the characteristics of the *in vivo* counterpart will address the call for development of appropriate tissue models that will reduce and/or refine animal experiments. There is extensive interest by the pharmaceutical industry in *in vitro* methods that will help meet the requirements of pending European Union legislation related to the testing of chemicals and xenobiotic absorption (36).

Even though cell lines have long been an integral part of drug discovery and development, cell line-based assays have limitations (4). For instance, the Caco-2 monolayers form a non-physiological barrier compared to the *in vivo* human small intestine, weakly express important intestinal metabolic enzymes such as CYP3A (9), and do not provide accurate results for carrier-mediated transport (12). MDCK cells have also been used for drug absorption studies but these cells are canine-derived kidney cells that weakly express P-gp (5), which limits their utility as a model for human intestinal drug transport. Cell lines with non-physiological barriers may lead to the use of inappropriate clinical dose regimens resulting in false negatives or elevated toxicity (37). As presented herein, P_{app} values for the SMI microtissues correlated with human absorption to a higher degree than did P_{app} values for the Caco-2 monolayers (Fig. 9). Furthermore, preliminary experiments showed the functionality of the drug metabolizing enzymes expressed on the intestinal microtissues (Table VIII) and Fig. 11. The results in Fig. 11 parallel other results that showed CYP3A, CYP2C9, and CYP2C19 are expressed in the rat small intestine with expression levels of 80%, 14%, and 2%, respectively (38). Since drug metabolism plays a significant role in the delivery of bioactive drug into the blood-stream, the preliminary metabolism results presented herein point to another advantage of the SMI microtissues in screening drug absorption at an early stage of drug development. The new, primary human cell-based 3-D small intestinal (SMI) microtissues will avoid the deficiencies noted for cell lines. The

Author Manuscript Author Manuscript Author Manuscript Author Manuscript

microtissues will provide pharmaceutical scientists with a reproducible model that more accurately recapitulates the physiological barrier and transport properties of native human intestinal tissue. *In vitro* models that express drug transporter proteins and metabolizing enzymes are vital to the pharmaceutical industry for screening of drug candidates since they directly affect bioavailability of drugs (5).

As the aging population increases, a growing number of individuals are simultaneously exposed to multiple medications. In order to reduce unintended consequences of drug-drug interactions (DDI), the FDA recommends inclusion of *in vitro* studies to determine whether a drug is a potential substrate or inhibitor of transporters such as P-gp or BCRP during the preclinical phase of drug development (39). Drug exposure changes due to DDI can lead to drug toxicity or lack of efficacy, particularly for drugs with narrow therapeutic index (6). Early prediction of drug candidates for intestinal permeability could also be important for dosage adjustment and therapeutic monitoring to mitigate risk (39). In this study, we have shown the utility of the intestinal microtissues for predicting DDI. Inhibitors of drug transporters increased the permeability of substrates and decreased the efflux ratio (elimination) which *in vivo* will affect drug bioavailability (Table VII and Fig. 10). The use of intestinal microtissues to predict DDI will bring added translational value to reduce undesired GI ADR resulting from the interaction between investigational and existing drugs.

As shown in Fig. 9a, b, permeation results for the SMI microtissues correlated better with human absorption data ($r^2 = 0.91$) compared to Caco-2 cells ($r^2 = 0.71$). Although the mechanisms of compound permeation through intestinal tissue are not completely understood, we believe that the improved correlation of the SMI microtissues is due to at least three factors including their *in vivo*-like: A) Structure B) Barrier properties, and C) Expression of transporters and metabolizing enzymes. A) Structure: As shown in Figs. 2, 3, 4 and 5, the structure of SMI microtissues closely parallels that of native intestinal tissue. The well polarized geometry, formation of villi, microvilli, and tight junctions, and localization of drug transporters and drug metabolizing enzymes, all mimic that of *in vivo* intestinal tissue. Further, the intestinal microtissues have well developed villi-like structure (Fig. 3) which increases the surface area for drug absorption similar to the *in vivo* situation. The presence of villi and microvilli on intestinal epithelium increases the surface area of tissues significantly compared to flat surfaces. In contrast, many of these features are lacking in Caco-2 cells or they do not parallel that of the *in vivo* tissue. B) Barrier properties: Paracellular transport is controlled by tight junctions present between cells in the intestinal epithelium and Caco-2 cells have elevated barrier properties with TEER ranging from 250 to 2400 $\Omega*cm^2$ compared to 12–120 $\Omega*cm^2$ for human small intestinal tissue. TEER values for the SMI microtissues were 152.5 ± 39 $\Omega*cm^2$ ($n = 33$ experiments) which is much closer to native barrier properties. C) Expression of transporters and drug metabolizing enzymes: Transcellular transport within intestinal tissue occurs with the assistance of both uptake and efflux transporters. Likewise, the effect of drug metabolizing enzymes has a significant effect on the permeability of parent drug through the intestinal tissue. Caco-2 cells under-express transporters and metabolizing enzymes compared to *in vivo* counterpart (40, 41). As shown in Tables II, III, IV, and VIII, the SMI microtissues express intestinal drug metabolizing enzymes and drug transporters at levels similar to those of the *in vivo* intestinal tissue. Hence, the higher correlation between permeation results for the SMI microtissues

Author Manuscript Author Manuscript Author Manuscript Author Manuscript

and human absorption data versus those for Caco-2 cells is likely a combination of the structure, barrier properties, and expression of key transporters and enzymes, all of which the SMI microtissues more closely recapitulate.

The reconstructed intestinal microtissues will provide significant benefits to the pharmaceutical industry by providing a model with: 1) polarity and defined structural geometry that allows for topical ("luminal side") or basolateral ("systemic") application of drugs to study lumen to bloodstream (A → B) or bloodstream to lumen (B → A) drug transport; and 2) wall-to-wall growth in tissue culture inserts that allows direct quantification of *in vivo*-like epithelial barrier integrity (e.g. using TEER). The drug permeability model utilizing the SMI microtissues correlates well with human *in vivo* absorption for compounds selected from different categories of the BCS classification. The format of the newly developed SMI microtissues allows simultaneous assessment of drug permeation, drug-drug interaction, drug metabolism, and toxicity (safety). In addition, important information related to other responses such as inflammation or drug-induced injury and repair can be monitored using the SMI microtissues. The ability to maintain the microtissues in culture for a 6-week period is anticipated to provide significant utility in studying drug induced injury to the GI tract, a common problem in repeat dose therapeutic regimens (e.g. cancer treatment). SMI microtissues have also been used to elucidate the effects of extended drug exposure (28–30 days) in a liver-intestine microphysiological co-culture system (16, 42). However, like other 3D tissue models, the small intestinal microtissues have limitations in that they may not represent the different cellular complexity of native tissues and they lack vascularization. In addition, a more complete evaluation of the metabolic activity of the SMI microtissues is needed. Finally, tissues such as lab-to-lab reproducibility and validation of the microtissues need to be addressed.

Conclusion

The 3D small intestinal microtissues structurally and functionally mimic the *in vivo* counterpart and provide a reproducible *in vitro* testing tool to predict the bioavailability of orally administered drug compounds. The availability of a reliable primary human cell-based intestinal tissue model will narrow the knowledge gap between 2D–based assays and *in vivo* drug absorption studies and improve the translation of *in vitro* results to the clinic. Nonetheless, additional studies utilizing a larger set of model drugs from different chemical classes and interlaboratory validation studies are needed to further establish the utility of the intestinal microtissue model for drug permeation studies. In addition to predicting drug absorption, we anticipate that the reconstructed SMI microtissues will have utility in studies aimed at elucidating: a) drug-induced gastrointestinal (GI) toxicity (43, 44) under acute and extended exposure conditions, b) GI inflammation, c) innate immune responses, d) GI tract infection (45), e) effects of probiotics (46), and f) disease modeling.

In summary, this study presents a novel *in vitro* SMI microtissue model which is reproducible, cost effective and which more closely resembles *in vivo* human tissue compared to other available models. The human primary cell-based intestinal 3D microtissues will provide researchers with a valuable tool for predicting drug absorption in

Author Manuscript Author Manuscript Author Manuscript Author Manuscript

the GI tract. The new microtissues are anticipated to reduce cost for compound screening and decrease the number of animals used for drug permeation studies.

ACKNOWLEDGMENTS AND DISCLOSURES

Research reported in this publication was supported by the National Institute of General Medical Sciences of the National Institutes of Health under Award Number R44GM108164. We thank Cyprotex for the LC-LC/MS work. Our thanks are extended to Drs Nathalie Chauret and Marc-Oliver Boily (Vertex Pharmaceutical, Canada) for their help in the metabolism data. We also would like to thank Bill Fowie (Northeastern University, Boston, MA) for performing the scanning electron microscopy work.

ABBREVIATIONS

Ω	Ohm
2D	Two dimensional
3D	Three dimensional
Å	Angstrom
(A)	Apical
ABCB1	ATP binding cassette subfamily B member 1
ABCC1	ATP Binding Cassette Subfamily C Member 1
ABCC2	ATP Binding Cassette Subfamily C Member 2
ABCG2	ATP-binding cassette sub-family G member 2
ADR	Adverse drug reaction
ALI	Air–liquid interface
(B)	Basolateral
BCRP	Breast cancer resistance protein
BCS	Biopharmaceutical Classification System
CDCF	5(6)-carboxy-2′,7′-dichlorofluorescein(CDCF)
cDNA	Complementary DNA
CK	Cytokeratin
Cq	PCR cycles
Ct	Threshold cycle
CYP450	Cytochrome P450
DDI	Drug-drug interaction
FDA	Food and Drug Administration

Author Manuscript Author Manuscript Author Manuscript Author Manuscript

FT	Full-thickness
GAPDH	Glyceraldehyde-3-phosphate dehydrogenase
GI	Gastrointestinal
HPLC	High performance liquid chromatography
H	Hour
IIAM	International Institute for the Advancement of Medicine
LC/MS	Liquid chromatography–mass spectrometry
LY	Lucifer Yellow
MDCK	Madin-Darby canine kidney
MDR1	Multi-drug resistance gene (MDR)-1
Met	Metabolite
Min	Minutes
MRP-1	Multidrug-resistance associated protein-1
MRP-2	Multidrug-resistance associated protein-2
MS MRM	Mass spectroscopy multiple reaction monitoring
MTT	3-(4,5-dimethylthiazole-2-yl)-2,5-diphenyl tetrazolium bromide
OPO	Organ Procurement Organization
$\mathbf{P_{app}}$	Apparent permeability coefficient
P-gp	p-Glycoprotein
PR	Parental
PT	Partial thickness
qPCR	Quantitative polymerase chain reaction
RFU	Relative fluorescence unit
RNA	Ribonucleic acid
RT	Room temperature
RT-PCR	Reverse Transcription Polymerase Chain Reaction
SEM	Scanning electron microscopy
SMI	Small intestine
TEER	Transepithelial electrical resistance

Author Manuscript Author Manuscript Author Manuscript Author Manuscript

TEM	Transmission electron microscopy
TTT	TEER of treated tissues
TUT	TEER of untreated tissues

REFERENCES

1. Pretorius E, Bouic PJD. Permeation of four oral drugs through the human intestinal mucosa. AAPS PharmSciTech. 2009;10:270–5. [PubMed: 19280345]
2. Brendon M, Baker BM, Christopher S, Chen CS. Deconstructing the third dimension – how 3D culture microenvironments alter cellular cues. J Cell Sci. 2012;125:3015–24. [PubMed: 22797912]
3. Loriot Y, Perlemuter G, Malka D, Penault-Llorca F, Boige V, Deutsch E, et al. Drug insight: gastrointestinal and hepatic adverse effects of molecular-targeted agents in cancer therapy. Nat Clin Pract Oncol. 2008;5:268–78. [PubMed: 18349858]
4. Hubatsch I, Ragnarsson EGE, Artursson P. Determination of drug permeability and prediction of drug absorption in Caco-2 monolayers. Nat Protoc. 2007;2:2111–9. [PubMed: 17853866]
5. Lee MKK, Dilq. Drug development in cell culture: crosstalk from the industrial prospects. J Bioequivalence Bioavailab. 2014;6:O96–O114.
6. Volpe DA. Drug-permeability and transporter assays in Caco-2 and MDCK cell lines. Future Med Chem. 2011;3:2063–77. [PubMed: 22098353]
7. Gupta V, Doshi N, Mitragotri S. Permeation of insulin, calcitonin, and exenatide across Caco-2 monolayers: measurement using rapid 3-day system. PLoS One. 2013;8:e77136. [PubMed: 24155924]
8. Tavelin S, Taipalensuu J, Söderberg L, Morrison R, Chong S, Artursson P. Prediction of the oral absorption of low permeability drugs using small intestine-like 2/4/A1 cell monolayers. Pharm Res. 2003;20:397–405. [PubMed: 12669959]
9. Ferrec EL, Chesne C, Artusson P, Brayden D, Fabre G, Gires P, et al. In vitro models of the intestinal barrier. The report and recommendations of ECVAM workshop 46. ATLA. 2001;29:649–68. [PubMed: 11709041]
10. Huang Y, Adams MC. An in vitro model for investigating intestinal adhesion of potential dairy propionibacteria probiotic strains using cell lineC2BBe1. Lett Appl Microbiol. 2003;36:213e216. [PubMed: 12641713]
11. Fang Y, Eglen RM. Three-dimensional cell cultures in drug discovery and development. SLAS Disc. 2017;22:456–72.
12. Mathur A, Loskill P, Shao K, Huebsch N, Hong SG, Marcus MG, et al. Human iPSC-based cardiac microphysiological system for drug screening applications. Sci Rep. 2017;5:8883.
13. Li AP. Preclinical in vitro screening assays for drug-like properties. Drug Discov Today. 2005;2:179–85.
14. Amdion GL, Lennerlas H, Shah VP, Crison JR. A theoretical basis for biopharmaceutics drug classification: the correlation of in vitro drug product dissolution and in vivo drug bioavailability. Pharm Res. 1995;12:413–20. [PubMed: 7617530]
15. http://www.fda.gov/downloads/Drugs/GuidanceComplianceRegulatoryInformation/Guidances/ucm072101.pdf.
16. Maschmeyer I, Hasenberg T, Jaenicke A, Lindner M, Lorenz AK, Zech J, et al. Chip-based human liver-intestine and liver-skin co-cultures-a first step toward systemic repeated dose substance testing in vitro. Eur J Pharm Biopharm. 2015;95:77–87. [PubMed: 25857839]
17. Wang Z, Hop CE, Leung KH, Pang J. Determination of in vitro permeability of drug candidates through a caco-2 cell monolayer by liquid chromatography/tandem mass spectrometry. J Mass Spectrom. 2000;35:71–6. [PubMed: 10633236]
18. Mosmann T Rapid calorimetric assay for cellular growth and survival: application to proliferation and cytotoxicity assays. J Immunol Methods. 1983;65:55–63. [PubMed: 6606682]

Author Manuscript Author Manuscript Author Manuscript Author Manuscript

19. Ito S, Karnovsky MJ. Formaldehyde-glutaraldehyde fixative containing trinitro compounds. J Cell Biol. 1968;39:168–169-A.
20. Zimmermann C Expression of drug transporters in intestine and blood. 2005 Doctoral thesis. http://edoc.unibas.ch/213/1/DissB_7139.pdf.
21. Rubas W, Jezyk N, Grass GM. Comparison of the permeability characteristics of a human colonic epithelial (Caco-2) cell line to colon of rabbit, monkey, and dog intestine and human drug absorption. Pharm Res. 1993;10:113–8. [PubMed: 8430047]
22. Shugarts S, Benet L. The role of transporters in the pharmacokinetics of orally administered drugs. Pharm Res. 2009;26:2039–54. [PubMed: 19568696]
23. Christians U Transport proteins and intestinal metabolism; P-glycoprotein and cytochrome P450 (CYP)-3A. Ther Drug Monit. 2004;26:104–6. [PubMed: 15228147]
24. Szarka CE, Pleiffer GR, Hum ST, Everley LC, Baishem AM, Moore DF, et al. Glutathione S-transferase activity and glutathione s-transferase μ expression in subjects with risk for colorectal cancer. Cancer Res. 1995;55:2789–93. [PubMed: 7796404]
25. https://www.fda.gov/downloads/Drugs/Guidances/ucm070246.pdf.
26. Zhao Y, Le J, Abraham MH, Hersey A, Eddershaw PJ, Luscombe CN, et al. Evaluation of human intestinal absorption data and subsequent derivation of a quantitative structure activity-relationship (QSAR) with the Abraham descriptors. J Pharm Sci. 2001;90:749–83. [PubMed: 11357178]
27. Shirasaka Y, Kuraoka E, Spahn-Langguth H, Nakanishi T, Langguth P, Tamai I. Species difference in the effect of grapefruit juice on intestinal absorption of Talinolol between human and rat. J Pharmacol Exp Ther. 2010;332:181–9. [PubMed: 19779132]
28. Bock U, Flototto T, Haltner E. Validation of cell culture models for the intestine and the blood-brain barrier and comparison of drug permeation. ALTEX. 2004;21(Suppl 3):57–64. [PubMed: 15057409]
29. Zaki NM, Artursson P, Bergström C. A modified physiological BCS for prediction of intestinal absorption in drug discovery. Mol Pharm. 2010;7:1478–87. [PubMed: 20734997]
30. Kiela PR, Ghishan FK. Physiology of intestinal absorption and secretion. Best Pract Res Clin Gastroenterol. 2016;30:145–59. [PubMed: 27086882]
31. Crawley SW, Mooseker MS, Tyska MJ. Shaping the intestinal brush border destruction by enterohemorrhagic Escherchia coli (EHEC): new insights from organoid culture. J Cell Biol. 2014;207:441–51. [PubMed: 25422372]
32. Holmes R, Lobley RW. Intestinal brush border revisited. Gut. 1998;30:1667–78.
33. Tyska MJ. Brush border destruction by enterohemorrhagic Escherchia coli (EHEC): new insights from organoid culture. Cell Mol Gastroenterol Hepatol. 2016;2:7–8. [PubMed: 28174702]
34. Engler AJ, Sen S, Sweeney HL, Discher DE. Matrix elasticity directs stem cell lineage specification. Cell. 2006;126:677–89. [PubMed: 16923388]
35. Gilbert PM, Havenstrite KL, Magnusson KEG, Sacco A, Leonardi NA, Kraft P, et al. Substrate elasticity regulates skeletal muscle stem cell self-renewal in culture. Science. 2010;329:1078–81. [PubMed: 20647425]
36. Srinivasan B, Kolli AR, Esch MB, Abaci HE, Shuler ML, Hickma JJ. TEER measurement techniques for in vitro barrier model systems. J Lab Autom. 2015;20:107–26. [PubMed: 25586998]
37. Balimane PV, Han Y-H, Chong S. Current industrial practices of assessing permeability and p-glycoprotein interaction. AAPS J. 2006;8:E1–E13. [PubMed: 16584115]
38. Hersman EM, Bumpus NN. A targeted proteomics approach for profiling murine cytochrome P450 expressions. J Pharmacol Exp Ther. 2014;349:221–8. [PubMed: 24594750]
39. US FDA. Guidance for industry drug interaction studies — study design, data analysis, implications for dosing, and labeling recommendations. 2006 https://www.fda.gov/OHRMS/DOCKETS/98fr/06d-0344-gdl0001.pdf.
40. DiMarco RL, Hunt DR, Dewi RE, Heilshorn SC. Improvement of paracellular transport in the Caco-2 drug screening model using protein-engineered substrates. Biomaterials. 2017;129:152–62. [PubMed: 28342321]

Author Manuscript Author Manuscript Author Manuscript Author Manuscript

41. Cummins CL, Mangravite LM, Benet LZ. Characterizing the expression of CYP3A4 and efflux transporters (P-gp, MRP1, and MRP2) in CYP3A4-transfected Caco-2 cells after induction with sodium butyrate and the phorbol ester 12-O-tetradecanoylphorbol-13 acetate. Pharm Res. 2001;18:1102–9. [PubMed: 11587480]
42. Maschmeyer I, Lorenz AK, Schimek K, Hasenberg T, Ramme AP, Hubner J, et al. A four-organ-chip for interconnected long-term co-culture of human intestine, liver, skin and kidney equivalents. Lab Chip. 2015;15:2688–99. [PubMed: 25996126]
43. Car D, Ayehunie S, Davies A, Duckworth C, French S, Hall N, et al. Towards better modeling and mechanistic biomarkers for drug-induced gastrointestinal injury. Pharmacol Ther. 2017;172:181–94. [PubMed: 28132905]
44. Eaton AD, Zimmermann Delaney CB, Hurley BP. Primary human polarized small intestinal epithelial barriers respond differently to a hazardous and an innocuous protein. Food Chem Toxicol. 2017;106:70–7. [PubMed: 28533127]
45. Maldonado-Conteras A, Birtley JR, Boll E, Zhao Y, Mumy KL, Toscano J, et al. Shigella depends on SepA to destabilize the intestinal epithelial integrity via cofilin activation. Gut Microbes. 2017;8: 544–60. [PubMed: 28598765]
46. Anselmo AC, McHugh KJ, Webster J, Langer R, Jaklenec A. Layer-by-layer encapsulation of probiotics for delivery to the microbiome. Adv Mater. 2016;28:9486–90. [PubMed: 27616140]

Author Manuscript Author Manuscript Author Manuscript Author Manuscript

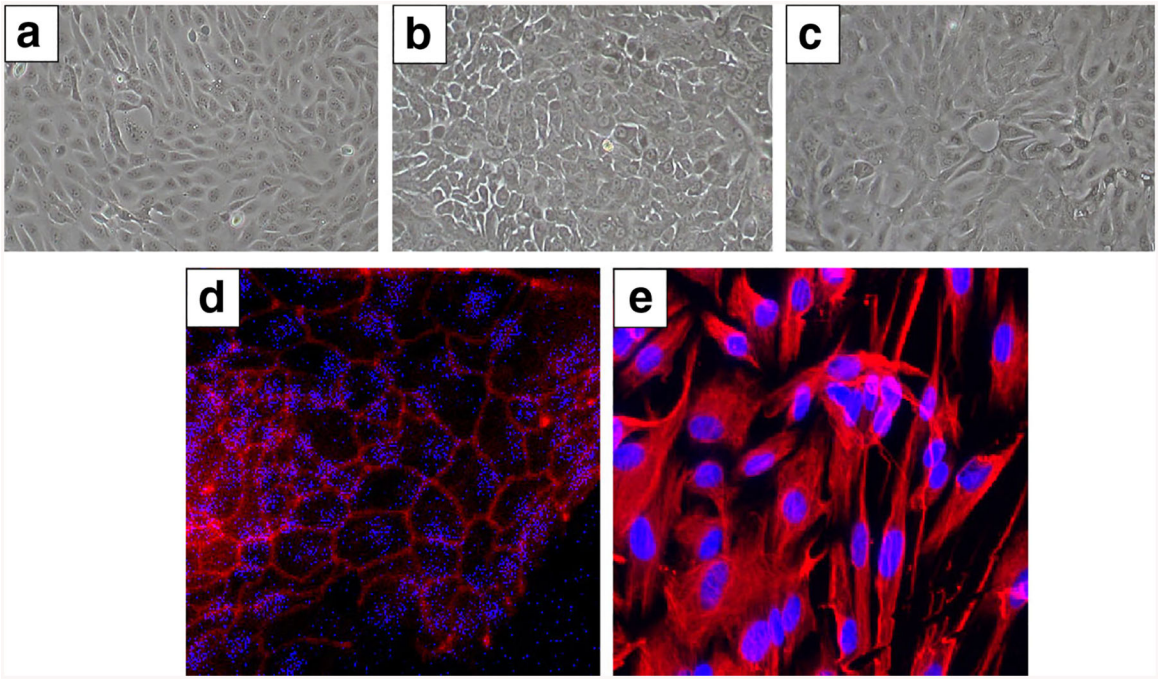

Fig. 1.

Monolayer culture of primary human small intestinal cells harvested from the: (**a**) duodenum, (**b**) jejunum, and (**c**) ileum of primary human small intestine tissue. Epithelial cells were stained for the epithelial tight junction marker ZO-1 (**d**), and primary small intestine fibroblasts were stained with the fibroblast marker, Vimentin (**e**).

Author Manuscript Author Manuscript Author Manuscript Author Manuscript

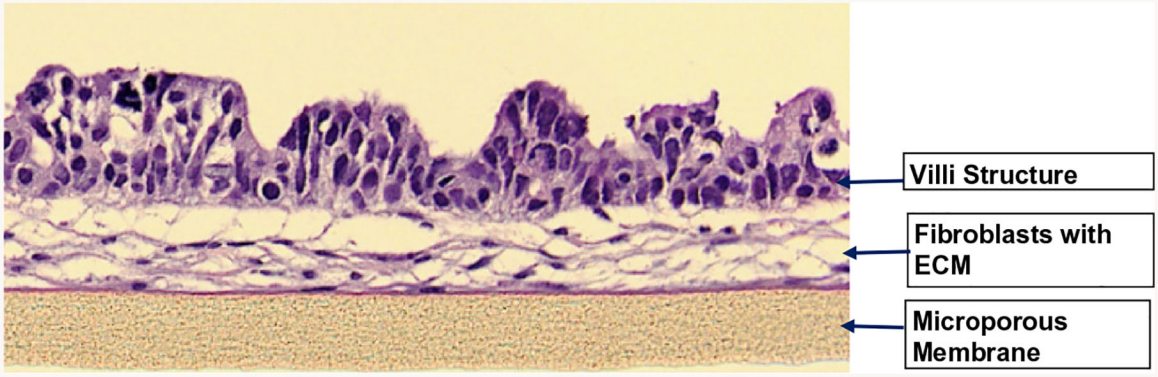

Fig. 2.

H&E stained histological cross-section of the small intestine microtissues showing the epithelium surface with villi, the basolateral fibroblast extracellular matrix substrate, and the underlying microporous membrane support (pore diameter = 0.4 um).

Author Manuscript Author Manuscript Author Manuscript Author Manuscript

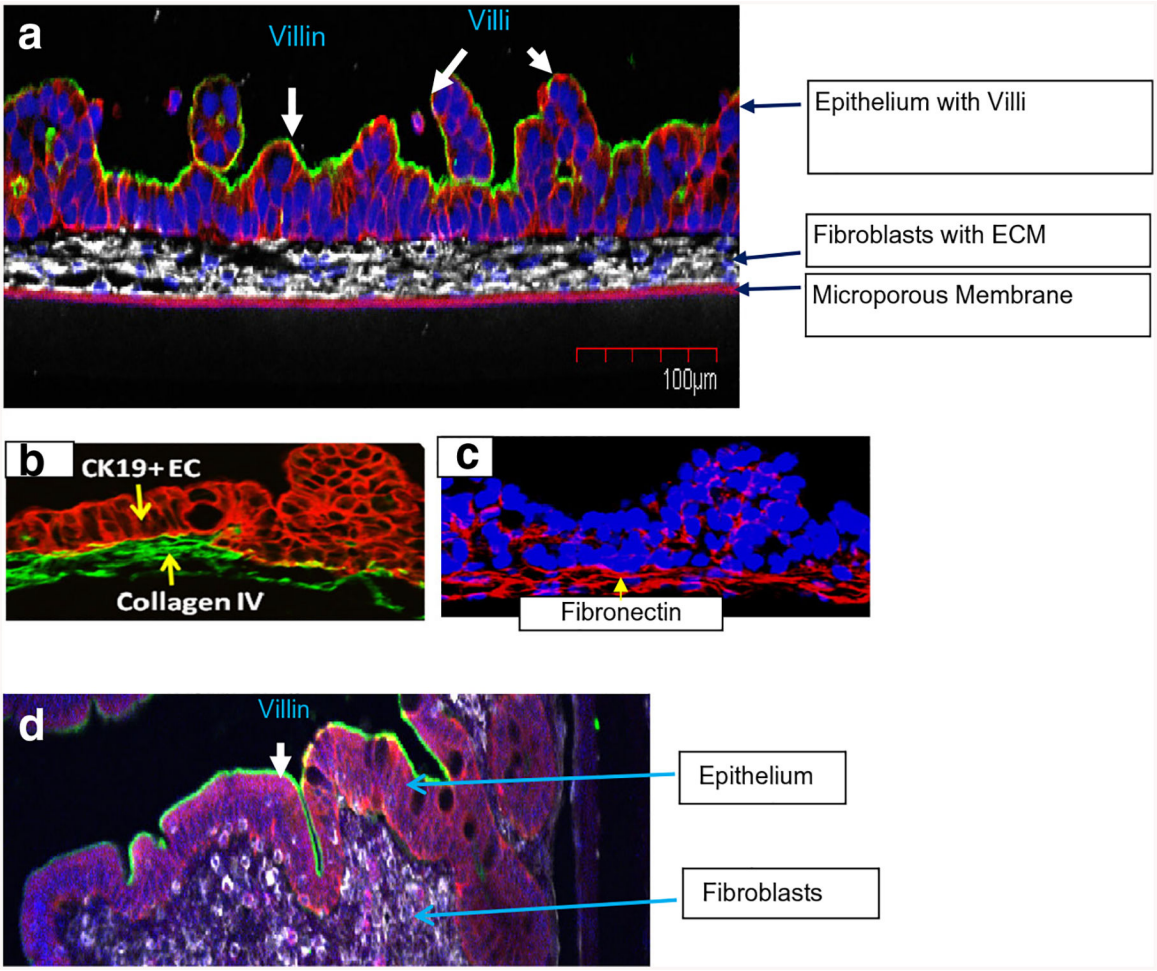

Fig. 3.

Immmuno-stained cross-sections of the *in vitro* reconstructed SMI microtissues showing cytokeratin (CK)-19 stained columnar epithelial cells (red), villin stained apical surface of epithelium (marker for brush border, green) and vimentin stained fibroblasts in the underlying ECM substrate (white). Additional images show de novo synthesis of the extracellular matrix proteins, (**b**) collagen IV (green) and (**c**) fibronectin (red). Human explant small intestinal tissue control tissues stained for villin (green, apical surface), CK19 positive epithelium (red) and fibroblasts (white) are shown (**d**). Nuclei were stained with DAPI (blue). EC = Epithelial cell layer.

Author Manuscript Author Manuscript Author Manuscript Author Manuscript

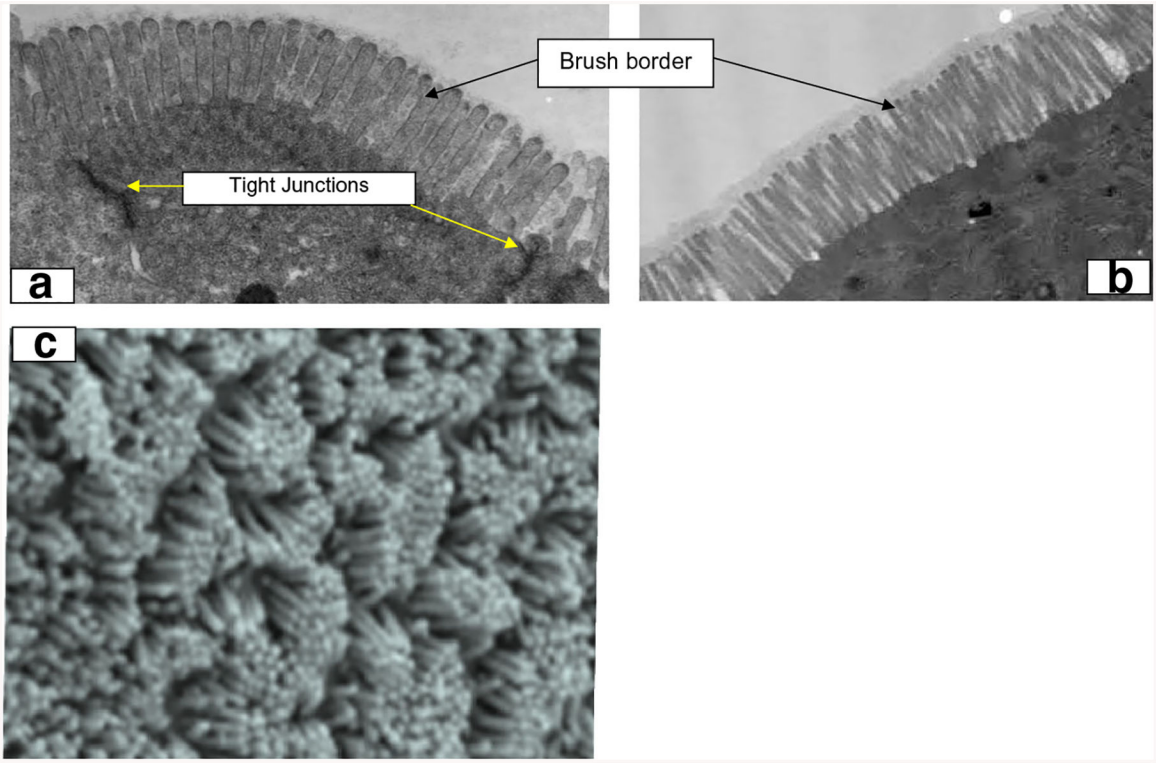

Fig. 4.

Transmission electron micrographs (TEM) of small intestine microtissues showing brush border membranes with tight junctions (TJ) in: (**a**) the SMI microtissues and (**b**) human intestinal explant tissue. Scanning electron microscopy (SEM) was used to visualize villi structures on the SMI microtissue surface (**c**).

Author Manuscript Author Manuscript Author Manuscript Author Manuscript

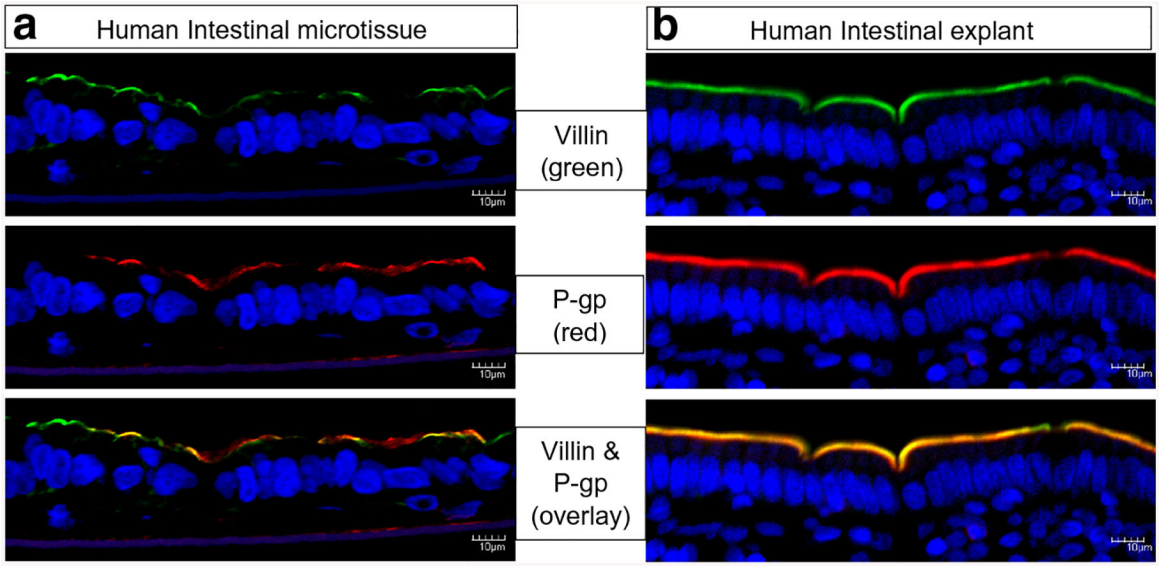

Fig. 5.

Immmuno-stained cross-sections of: (**a**) *In vitro* intestinal microtissues and (**b**) Human small intestine explant tissue. Both tissues express villin (marker of brush border), and the main drug transporter, P-glycoprotein (P-gp). An overlay of the villin and P-gp cross-sections show that both villin and P-gp are expressed on the apical surface of the *in vitro* and explant tissues.

Author Manuscript Author Manuscript Author Manuscript Author Manuscript

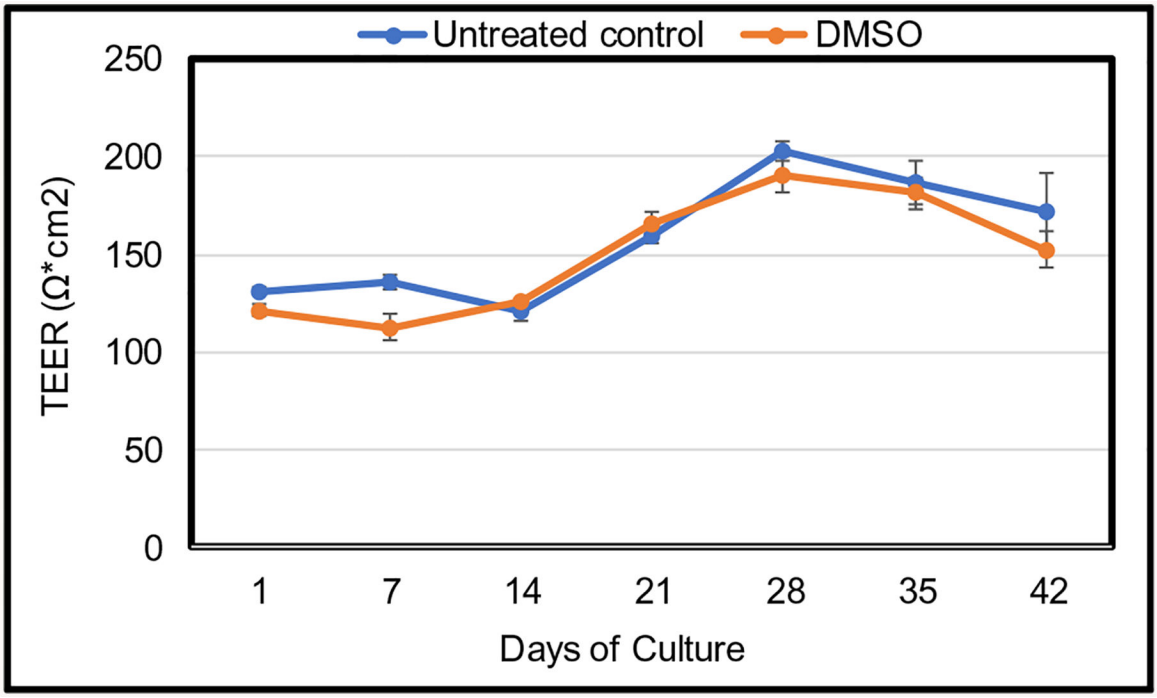

Fig. 6.

The effect of extended culture on the barrier properties of the SMI microtissues. As shown, TEER values remain constant over the 6-week experiment.

Author Manuscript Author Manuscript Author Manuscript Author Manuscript

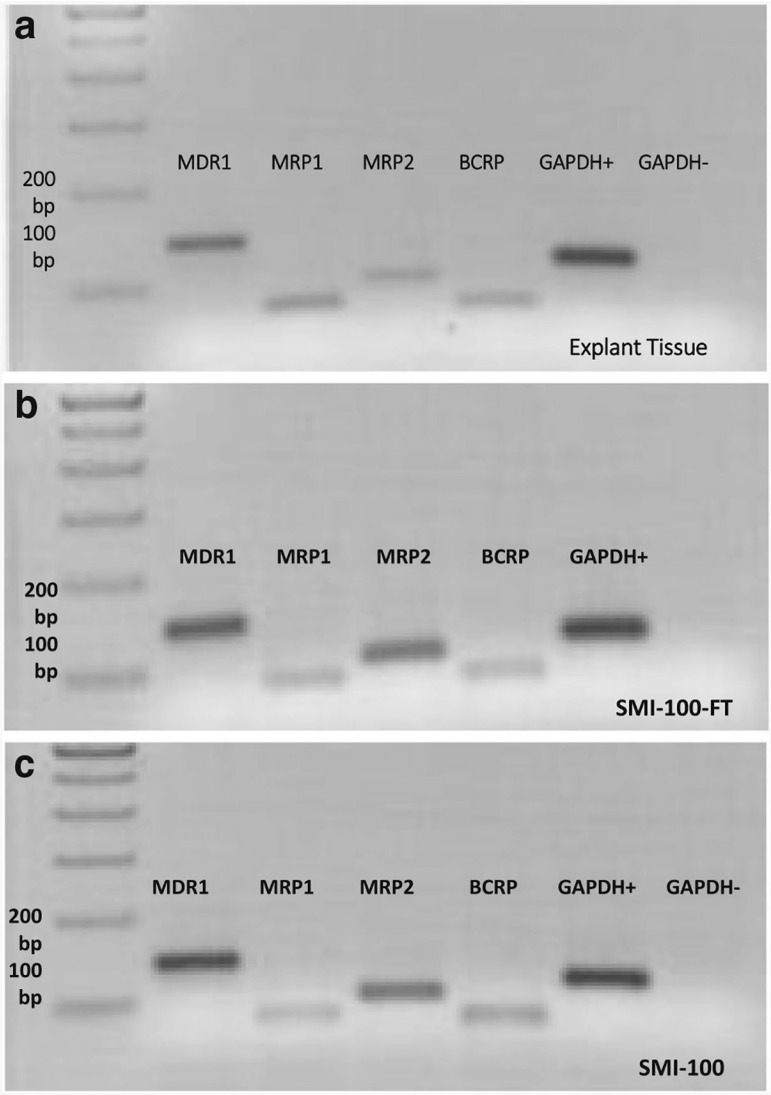

Fig. 7.

RT-PCR results showing gene expression of efflux transporters, P-glycoprotein (MDR1), BCRP, MRP1, and MRP2, by: (**a**) human small intestinal explant tissue, (**b**) full-thickness intestinal microtissues (SMI-FT; epithelial cells plus fibroblasts), and **c**) partial-thickness microtissues (SMI-PT; epithelial cells only).

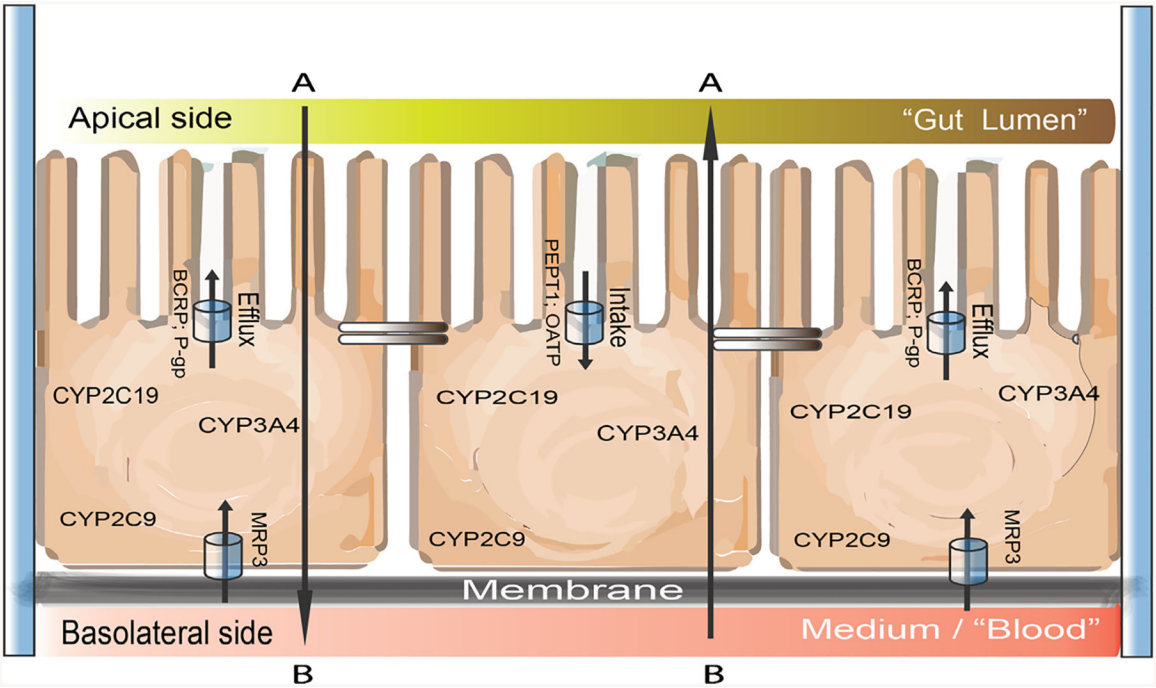

Fig. 8.

Schematic representation of small intestine tissue showing lumen side (apical) and blood side (basolateral) localization of drug metabolizing enzymes and drug transporters, and A-to-B and B-to-A transport of compounds.

Author Manuscript Author Manuscript Author Manuscript Author Manuscript

Author Manuscript Author Manuscript Author Manuscript Author Manuscript

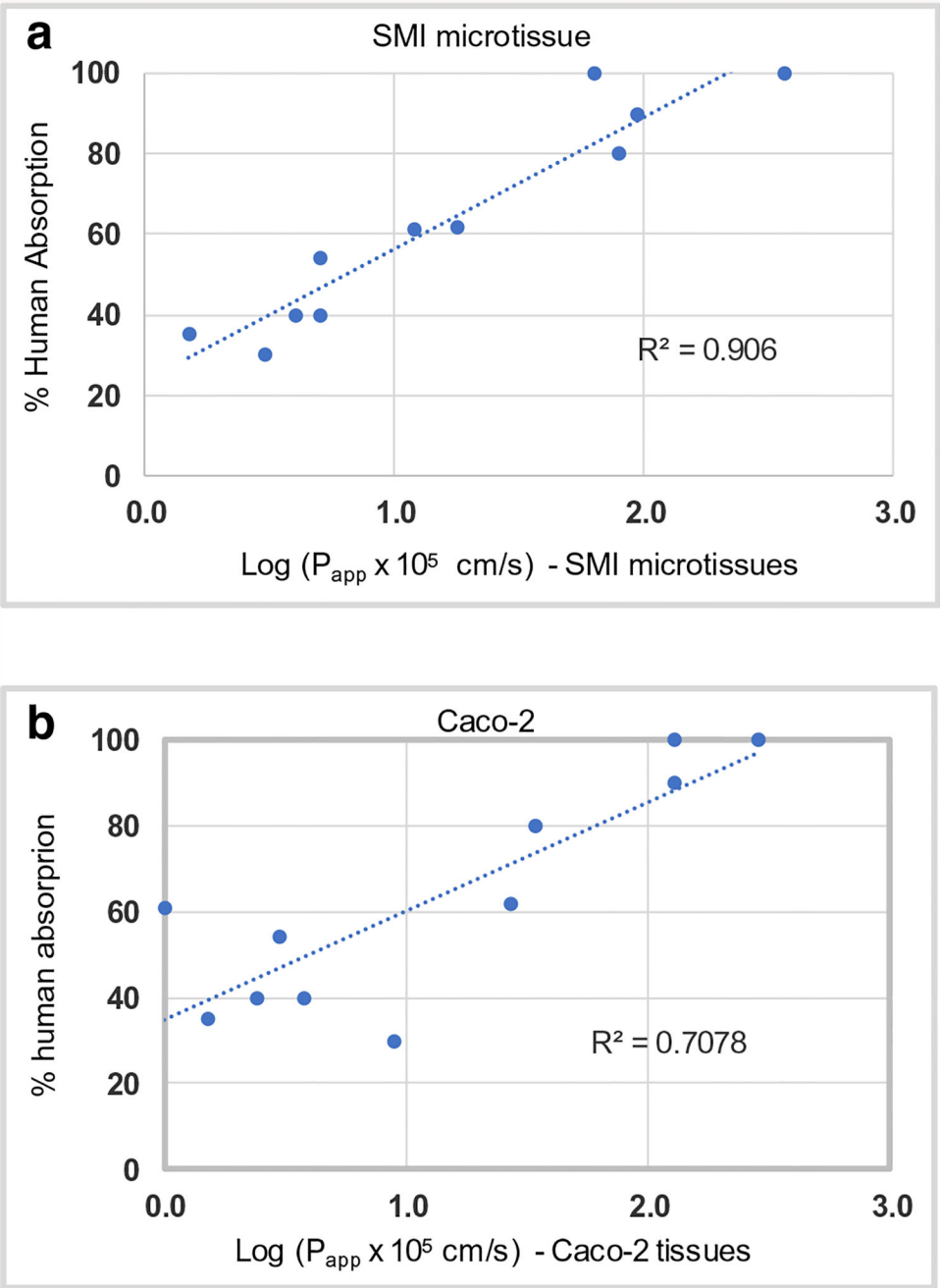

Fig. 9.

Correlation of human drug absorption with drug permeability results (P_{app}) for: (**a**) SMI-FT microtissues (and **b**) Caco-2 monolayers. Triplicate tissues were exposed to each model drug (n = 11) for 2 h. Average P_{app} values from two independent lots of SMI-FT microtissues were used.

Author Manuscript Author Manuscript Author Manuscript Author Manuscript

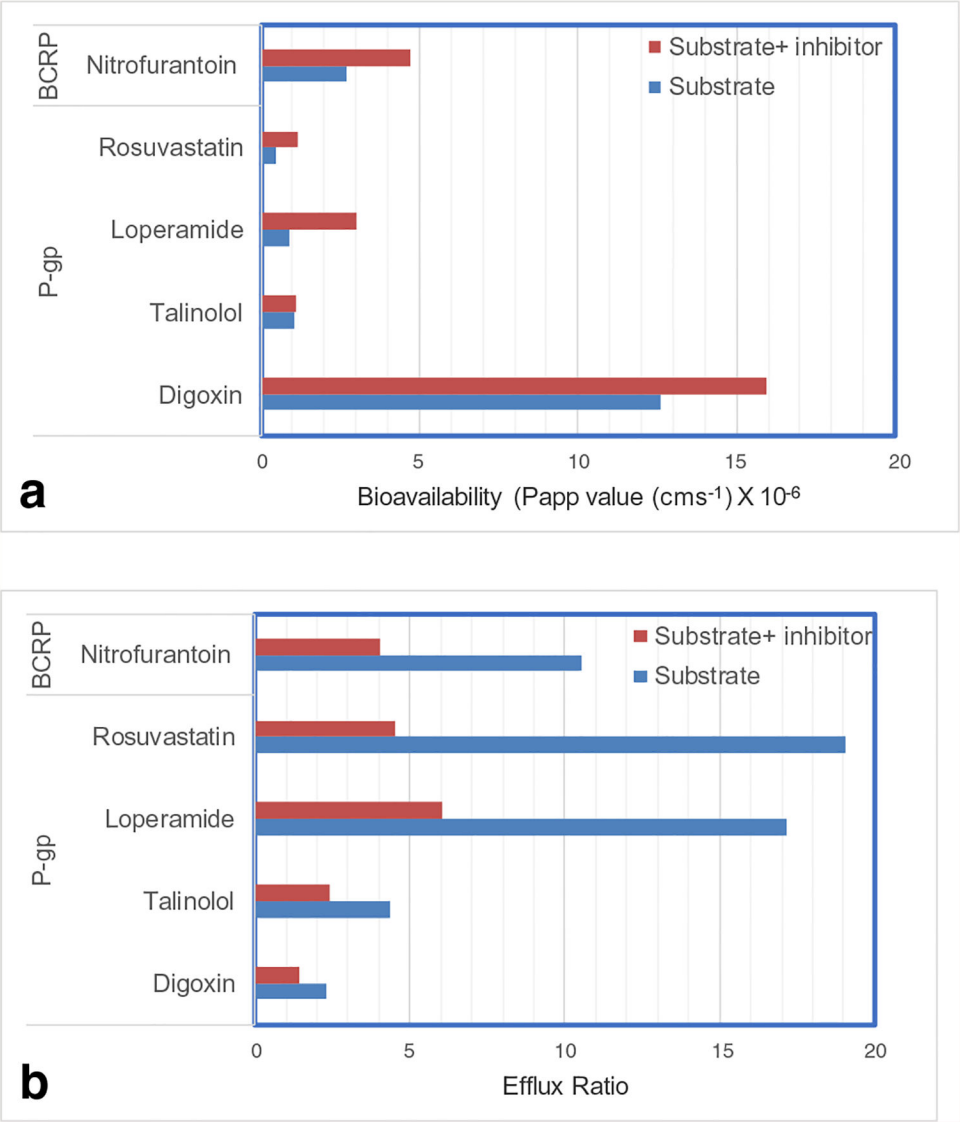

Fig. 10.

Effect of drug transporter inhibitors on drug permeation and the efflux ratio for the 3D intestinal microtissues. As shown, the presence of substrate inhibitors increases A→B permeability/bioavailability of the drug (**a**) and decreases the efflux ratio (**b**). P-gp substrates: Digoxin, Talinolol, Loperamide, and Rosuvastatin. BCRP substrate: Nitrofurantoin. P-gp inhibitor: Verapamil. BCRP inhibitor: Novobiocin.

Author Manuscript Author Manuscript Author Manuscript Author Manuscript

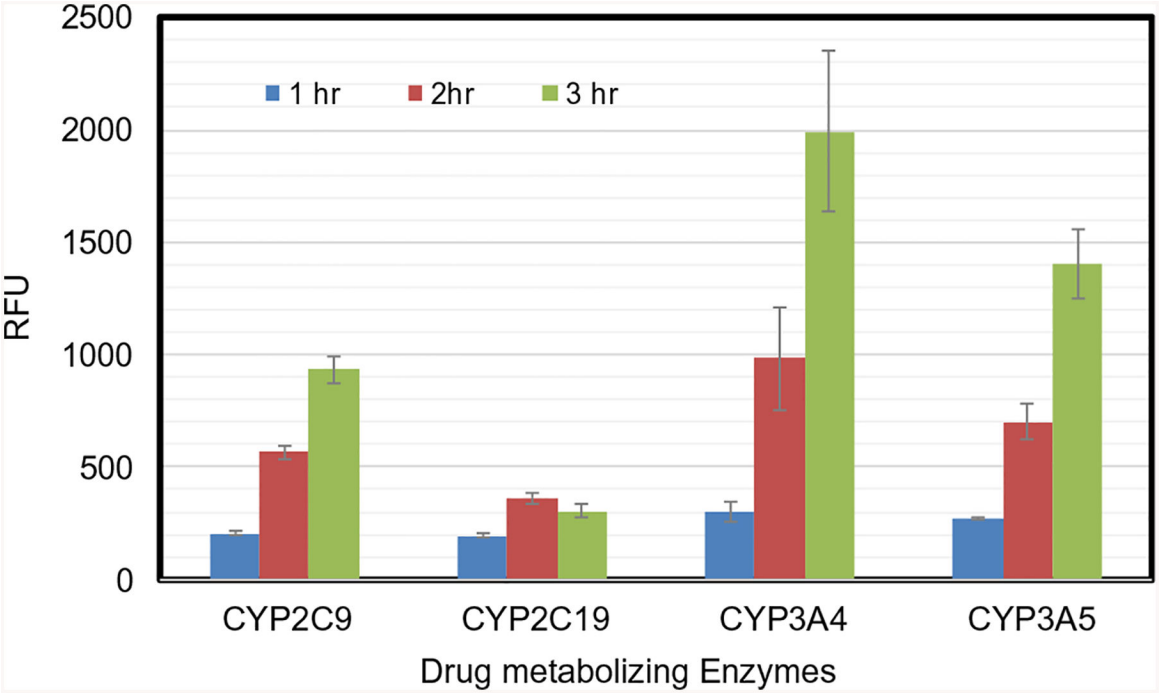

Fig. 11.

CYP450 enzyme metabolic activity of intestinal microtissues. Isozyme-specific substrates were applied to the small intestine microtissues and the metabolic activity was monitored using isozyme-specific fluorogenic substrates of CYP450 isozymes involved in drug metabolism. The CYP450 substrates are metabolized by a specific intestinal microtissue CYP450 enzyme and the products are highly fluorescent are released into the aqueous medium. The presence of fluorescent metabolites in the culture supernatants collected from the apical surfaces was measured after 1, 2, or 3 h. Fluorescent intensities were measured using a fluorescent plate reader.

Author Manuscript Author Manuscript Author Manuscript Author Manuscript

P-gp:	Forward	5`-CTGTATTGTTTGCCACCACGA-3`
	Reverse	5`-AGGGTGTCAAATTTATGAGGCAGT-3`
MRP1	Forward	5`-GGGCTGCGGAAAGTCGT-3`
	Reverse	5`-AGCCCTTGATAGCCACGTG-3`
MRP2	Forward	5`-ACTGTTGGCTTTGTTCTGTCCA-3
	Reverse	5`-CAACAGCCACAATGTTGGTCTCTA-3`:
BCRP	Forward	5`-CAGGTCTGTTGGTCAATCTCACA-3`
	Reverse	5`-TCCATATCGTGGAATGCTGAAG-3`

Author Manuscript Author Manuscript Author Manuscript Author Manuscript

Table I

Results from Viability (MTT) and Barrier Integrity (TEER and Lucifer Yellow Leakage) Assays Following Exposure of Model Drug Compounds to SMI Microtissues

				Barrier integrity				Tissue viability	
Compound	**Company**	**Catalogue #**	**Conc. (μM)**	**TEER**		**LY leakage**		**MTT**	
				TEER(%)	**CV (%)**	**LY Leakage (%)**	**CV(%)**	**Viability (%)**	**CV (%)**
Control				100.0	8.8	0.51	0.31	100.0	8.8
			1	84.6	5.3	0.55	0.23	104.0	9.2
Verapamil	Sigma	V4629	10	90.2	6.0	0.52	0.25	96.5	1.1
			100	93.4	4.5	0.42	0.34	92.5	2.0
			1	87.3	3.5	0.37	0.03	103.4	1.8
Propanolol	Sigma	P0884	10	93.2	2.1	0.55	0.10	102.7	1.0
			100	99.4	3.2	0.46	0.19	101.0	2.6
			1	99.1	3.3	0.00	0.00	100.4	2.2
Warfarin	Sigma	A2250	10	105.4	3.8	0.00	0.00	98.9	2.3
			100	100.4	1.1	0.00	0.00	92.9	3.5
			1	82.7	3.3	0.33	0.20	99.4	4.3
Quinidine	Sigma	Q3625	10	92.9	2.1	0.47	0.16	100.1	1.9
			100	97.2	3.2	0.46	0.12	99.3	3.4
			1	99.7	6.7	0.61	0.08	109.0	5.1
Enalapril	Sigma	E6888	10	97.3	17.0	0.66	0.14	104.6	11.8
			100	98.7	4.6	0.23	0.06	99.0	4.2
			1	97.7	18.0	0.36	0.20	108.2	6.3
Atenolol	Sigma	A7655	10	98.7	7.8	0.24	0.06	107.4	12.0
			100	94.2	6.0	0.71	0.10	102.5	4.1
			1	81.4	6.6	0.54	0.15	102.0	6.0
Ranitidine	Sigma	R101	10	90.5	2.6	0.64	0.03	98.1	1.9
			100	103.0	1.3	0.49	0.35	96.0	1.9
			1	103.0	9.2	0.47	0.09	109.4	8.5
Cimetidine	Sigma	C4522	10	92.1	3.1	0.34	0.29	103.2	15.5
			100	100.4	12.0	0.95	0.81	96.1	3.6

Author Manuscript Author Manuscript Author Manuscript Author Manuscript

Compound	Company	Catalogue #	Conc. (μM)	Barrier integrity				Tissue viability	
				TEER		LY leakage		MTT	
				TEER(%)	CV (%)	LY Leakage (%)	CV(%)	Viability (%)	CV (%)
			1	95.1	2.4	0.37	0.34	98.5	4.2
Acebutanol	Sigma	A3669	10	94.2	4.0	0.00	0.00	97.5	4.6
			100	91.6	6.6	0.41	0.48	1001.6	6.3
			1	91.4	3.7	0.29	0.30	102.6	4.2
Erythromycin	Sigma	E5389	10	96.4	1.5	0.08	0.11	100.1	2.1
			100	93.6	1.8	0.15	0.27	98.5	4.2
			1	93.5	6.7	0.28	0.14	104.0	2.9
Acyclovir	Sigma	PHR1254	10	94.6	9.1	0.27	0.12	97.6	3.4
			100	102.0	2.3	0.36	0.08	91.1	7.3

At each concentration, drugs were applied (at 0 and 48 h) topically and basolaterally to $n = 3$ microtissues for 96 h. Long term exposures were performed to monitor the maximum effect

Author Manuscript Author Manuscript Author Manuscript Author Manuscript

Table II

qPCR Results (RT^2 Profiler PCR Array Kit) Showing Phase I Drug Metabolizing Enzyme Gene Expression Levels for the SMI Microtissues Containing Intestinal Epithelial and Fibroblasts (SMI-FT) or Epithelial Cells Only (SMI-PT), and for Human Explant Tissue are Shown

Gene symbol	Gene description	RT^2 catalog number	Mean Cq			Fold change	
			Explant	SMI-PT	SMI-FT	SMI-PT	SMI-FT
CYP17A1	Cytochrome P450, family 17, subfamily A, polypeptide 1	PPH01226A	35.0	28.1	30.4	8.9	1.5
CYP1A1	Cytochrome P450, family 1, subfamily A, polypeptide 1	PPH01271F	35.0	28.0	26.2	9.4	29.7
CYP26A1	Cytochrome P450, family 26, subfamily A, polypeptide 1	PPH01229A	28.3	29.1	27.4	4.4	12.3
CYP2C19	Cytochrome P450, family 2, subfamily C, polypeptide 19	PPH01241C	27.6	25.3	25.4	0.4	0.3
CYP2C8	Cytochrome P450, family 2, subfamily C, polypeptide 8	PPH01235G	33.8	29.8	30.0	1.2	0.9
CYP2C9	Cytochrome P450, family 2, subfamily C, polypeptide 9	PPH00478B	27.5	26.7	27.0	0.1	0.1
CYP2S1	Cytochrome P450, family 2, subfamily S, polypeptide 1	PPH10710F	29.1	24.3	23.1	2.0	3.9
CYP3A4	Cytochrome P450, family 3, subfamily A, polypeptide 4	PPH01264A	25.7	25.6	24.7	0.1	0.1
CYP3A5	Cytochrome P450, family 3, subfamily A, polypeptide 5	PPH01219F	25.8	25.0	25.0	0.1	0.1
ESD	Esterase D	PPH20101A	27.1	23.0	23.1	1.3	1.0
ADH4	Alcohol dehydrogenase 4 (class II)	PPH01693F	29.9	26.5	25.3	0.8	1.5
ADH5	Alcohol dehydrogenase 5 (class III)	PPH01728A	27.3	23.9	23.5	0.8	0.9
ADH6	Alcohol dehydrogenase 6 (class V)	PPH20040B	29.1	27.6	28.4	0.2	0.1
ALDH1A1	Aldehyde dehydrogenase 1 family, member A1	PPH01723B	24.7	24.2	23.2	0.1	0.2
ALDH1B1	Aldehyde dehydrogenase 1 family, member B1	PPH20559A	32.5	28.2	28.1	1.5	1.4
ALDH2	Aldehyde dehydrogenase 2 family (mitochondrial)	PPH17047A	27.2	26.0	24.6	0.2	0.4

Author Manuscript Author Manuscript Author Manuscript Author Manuscript

Table III

qPCR Results (RT^2 Profiler PCR Array Kit) Showing Phase II Drug Metabolizing Enzyme Gene Expression Levels by the SMI Microtissues Containing Intestinal Epithelial and Fibroblasts (SMI-FT) and Human Explant Tissue are Shown

Symbol	Gene name	RT^2 catalog number	Mean Cq		Fold change SMI-FT
			Explant	SMI-FT	
ACSL3	Acyl-CoA synthetase long-chain family member 3	PPH15368F	29.37	25.17	7.01
ACSL4	Acyl-CoA synthetase long-chain family member 4	PPH15399A	29.46	26.2	3.66
CES1	Carboxylesterase 1	PPH60025F	27.45	22.98	8.46
CES2	Carboxylesterase 2	PPH15866B	29.06	26.11	2.95
COMT	Catechol-O-methyltransferase	PPH01584B	29.46	24.3	13.64
DDOST	Dolichyl-diphosphooligosaccharide-protein glycosyltransferase	PPH16500F	29.75	25.12	9.45
EPHX1	Epoxide hydrolase 1, microsomal (xenobiotic)	PPH01613F	28.86	26.06	2.66
GALNT1	polypeptide N-acetylgalactosaminyltransferase 1	PPH15641A	29.76	25.18	9.13
GSTA4	Glutathione S-transferase alpha 4	PPH01576B	29.48	26.65	2.71
GSTK1	Glutathione S-transferase kappa 1	PPH18961B	28.33	23.97	7.84
GSTO1	Glutathione S-transferase omega 1	PPH00867A	27.37	23.19	6.92
GSTP1	Glutathione S-transferase pi 1	PPH00318F	26.75	21.45	15.03
MGST2	Microsomal glutathione S-transferase 2	PPH01610E	29.05	24.97	6.45
NAA20	N(alpha)-acetyltransferase 20, NatB catalytic subunit	PPH01557F	29.37	25.16	7.06
SAT1	Spermidine/spermine N1 -acetyltransferase 1	PPH01303A	27.93	23.32	9.32

Author Manuscript Author Manuscript Author Manuscript Author Manuscript

Table IV

qPCR Data Showing Expression Levels of Drug Transporters in Partial Thickness (PT) and Full-Thickness (FT) Intestinal Microtissues

#	Gene name	Symbol	Mean Cq		Regulation (fold change)
			SMI-PT	SMI-FT	
	Glyceraldehyde-3-phosphate dehydrogenase	GAPDH	20.24 ± 0.01	21.28 ± 0.13	N/A
1	ATP-binding cassette, sub-family G (WHITE), member 2 (ABCG2)	BCRP	28.52 ± 0.09	29.84 ± 0.20	−1.25 ± 0.09
2	ATP-binding cassette, sub-family B (MDR/TAP), member 1 (ABCC1)	MRP1	29.35 ± 0.31	29.83 ± 0.21	1.42 ± 0.13
3	ATP-binding cassette, sub-family C (CFTR/MRP), member 2 (ABCC2)	MRP2	25.03 ± 0.46	25.73 ± 0.89	0.58 ± 1.47
4	ATP-binding cassette, sub-family B (MDR/TAP), member 1 (ABCB1)	P-gp/MDR1	29.85 ± 0.32	27.29 ± 0.36	11.79 ± 2.1

The fold change in expression levels between PT and FT (N = 3 runs) are indicated for each transporter

N/A = Not Applicable

Author Manuscript Author Manuscript Author Manuscript Author Manuscript

Table V

Comparison of Drug Permeation in the SMI Microtissues and the Caco-2 Cell Monolayers for Three Model Drugs: 1) Talinolol = Low Permeability Drug, 2) Ranitidine = Moderate Permeability Drug but Poorly Absorbed in Caco-2 Cell Monolayers, c) Warfarin = High Permeability Drug

	In vitro P_{app} A- > B(10^{-6} cm^{s-1})		*In vivo*
Test compounds	**SMI microtissues**	**Caco-2 cells**	**Fraction absorbed (%) in humans**
Talinolol	0.8 ± 0.1	0.2 ± 0.2	54
Ranitidine	2.2 ± 0.5	0.2 ± 0.0	61
Warfarin	22.3 ± 0.5	27.8 ± 7.6	100

Mean P_{app} values from n = 2 SMI microtissue lots are presented

Author Manuscript Author Manuscript Author Manuscript Author Manuscript

Table VI

Comparison of Drug Permeation in the SMI Microtissues and the Caco-2 Cell Monolayers for 11 Model Drugs

	MS MRM transition (Ql >Q3)	HPLC retention time (min)	SMI tissue	Caco-2	Historical human data			
			SMI mean A- > B P_{app} (10^{-6} cm s^{-1})	Caco-2 mean A- > B P_{app} (10^{-6} cm s^{-1})	Fraction absorbed (%) in humans	BCS	Human absorption	Ref
Verapamil	455.0 m/z > 165 m/z	1.33	6.3 ± 3.7	12.8	100	I	High	(25, 27)
Propranolol	260.3 m/z > 116.2 m/z	1.20	9.4 ± 5.4	12.9	90	I	High	(27)
Warfarin	309.2 m/z > 163.1 m/z	1.56	36.7 ± 16.8	28.6	100	I	High	(25)
Quinidine	325.8 m/z > 81.3 m/z	0.98	7.9 ± 2.7	3.4	80	II	High	(25)
Enalapril	377.3 m/z > 234 m/z	1.19	0.4 ± 0.2	0.2	40	III	Low	(25)
Atenolol	267.0 m/z > 145 m/z	0.81	0.5 ± 0.2	0.3	50	III	Low	(25, 27)
Ranitidine	315.2 m/z > 176.2 m/z	0.83	1.2 ± 0.7	0.1	61	III	Low	(25)
Cimetidine	252.2 m/z > 95.1 m/z	0.80	1.9 ±0.2	2.7	62	III	Low	(25)
Erythromycin	734.0 m/z > 734.6 m/z	1.23	0.15 ± 0.1	0.2	35	III	Low	(25)
Acebutolol	337.1 m/z > 116.1 m/z	1.04	0.4 ± 0.1	0.4	40	III	Low	(25)
Acyclovir	225.7 m/z > 152 m/z	1.12	0.3 ± 0.2	0.9	30	III	Low	(25)

Metoprolol was used as high permeability marker. Metoprolol A->B P_{app} value was 7.3 ± 1.0

Author Manuscript Author Manuscript Author Manuscript Author Manuscript

Table VII

Drug-drug Interaction Studies Using the Small Intestine Microtissues

Transporter	Substrate	Inhibitor	Conc (uM)	Assay duration (hr)	Mean A- > B P_{app} (10^{-6} cm s^{-1})	Mean B- > A P_{app} (10−6 cm s−1)	Efflux ratio
PgP	Digoxin	No Inhibitor	10	2	12.6 ± 0.74	29.0 ± 5.0	2.3
		Verapamil	100	2	16.0 ± 1.75	22.6 ± 2.9	1.4
	Talinolol	No Inhibitor	10	2	0.75 ± 0.07	2.8 ± 0.0	3.9
		Verapamil	100	2	1.1 ± 0.0	2.7 ± 0.07	2.4
	Loperamide	No Inhibitor	10	2	0.9 ± 0.0	15.5 ± 4.6	16.7
		Verapamil	100	2	3.0 ± 1.0	18.2 ± 0	6.5
	Rosuvastatin	No Inhibitor	10	2	0.5 ± 0.07	9.4 ± 1.0	19.1
		Elacider	100	2	1.2.0 ± 0.08	5.3 ± 0.3	4.5
BCRP	Nitrofurantoin	No Inhibitor	10	2	2.7 ± 1.6	28.4 ± 3.3	10.7
		Novobiocin	50	2	4.7 ± 0.65	18.9 ± 1.0	4.0
MRP2	CDCF	No Inhibitor	10	2	0.002 ± 0.01	0.08 ± 0.02	34.7
		MK-571	100	2	0.05 ± 0.05	0.1 ± 0.03	1.5

n = 3 microtissues were topically dosed with 75 μl (topically) or 250 μl (basolaterally) of permeation buffer containing 10 μM of substrate alone or in combination with the inhibitor for 2 hr

Author Manuscript Author Manuscript Author Manuscript Author Manuscript

Table VIII

Metabolism of Midazolam and the Prodrug, Fosphenytion, by Drug Metabolizing Enzymes Expressed by Small Intestinal Microtissues

Parental (PR) drug	Enzyme involved	Transport	%PR recovery	Metabolite	% metabolite	A-B P_{app} ($\times 10^{-6}$ cm s^{-1}	Efflux
Midazolam	CYP3A4	A-B	78.5	Alpha-hydroxymidazolam	6.59	14.4	0.95
		B-A	70.2		1.56	13.7	
Fosphenytion	Alkaline Phosphatase	A-B	1.37	Phenytoin	57.16	12.3	0.31
		B-A	36.05		3.77	3.77	

Microtissues ($n = 3$) were topically dosed with each model drug (10 μM) topically or basolaterally for 2 h

Author Manuscript Author Manuscript Author Manuscript Author Manuscript

Table IX

Reproducibility of Drug Permeation for the Small Intestine Microtissues

Test article	Lot #1 Mean A- > B P_{app} (10^{-6} cm s^{-1})	Lot #2 Mean A- > B P_{app} (10^{-6} cm s^{-1})	Lot #3 Mean A- > B P_{app} (10^{-6} cm s^{-1})	Fraction absorbed (%) in humans
Atenolol	0.68 ± 0.19	0.6 ± 0.28	0.5 ± 0.3	54%; (Moderate)
Ranitidine	1.1 ± 0.58	1.1 ± 0.25	0.7 ± 0.09	61%; (Moderate)
Hydrochlorothiazi de	ND	2.3 ± 0.12	4.1 ± 0.23	71%; (Moderate)
Warfarin	48.5 ± 8.18	24.3 ± 0.86	19.9 ±3.45	100%; (High)

n = 3 tissues were topically dosed with model drugs (10 μM) for 2 h

ND Not Done